Master thesis and internship[BR]- Master's thesis : Improving the Conditioning of the Acoustic Subsystem and Source Terms in Multifluid Plasma Equations of State[BR]- Integration Internship

Auteur : Clotuche, Julien
Promoteur(s) : Hillewaert, Koen
Faculté : Faculté des Sciences appliquées
Diplôme : Master en ingénieur civil en aérospatiale, à finalité spécialisée en "aerospace engineering"
Année académique : 2022-2023
URI/URL : http://hdl.handle.net/2268.2/16754

Université de Liège - Faculté des Sciences Appliquées

ATFE0005-1 Master thesis and internship

Improving the Conditioning of the Acoustic Subsystem and Source Terms in Multifluid Plasma Equations of State

Travail de fin d'études réalisé en vue de l'obtention du grade de master "Ingénieur Civil en Aérospatiale" par CLOTUCHE Julien

Author :
Clotuche Julien
Masters in Aerospace Engineering

Supervisors :
Hillewaert Koen

Teachers :
Grigorios Dimitriadis
Dewallef Pierre

Advisors :
Corthouts Nicolas
Gangemi Giuseppe

Année académique 2022-2023

Abstract

This work is realised in the ForDGe software and is a step towards the development of a tool capable of modeling electric propulsion such as Hall effect thrusters. It shows how the change from a non-dimensionlisation scheme with single velocity scale to a species dependent velocity scale improves the performances of the ForDGe software in the context of plasma modeling. ForDGe uses the Discontinuous Galerkin method, which is a combination of the principles of Finite Element and Finite Volume Methods, in combination with a Runge-Kutta time integration scheme. To explore the performances of the new non-dimensionalisation two test cases are used: the sod shock tube test case with and without computation of the electric potential.

The improvements metrics are the precision of the results and the convergence rate of the linear solver used in the time integration scheme: GMRes. The precision improvement is measured in the balance of the non-dimensionalised variables and accuracy of the results as adjudicated by analytical solutions. The convergence rate is dependent on the clustering of the eigenvalues of the expanded Jacobian and its improvement is measured by the scattering of those eigenvalues. The test cases show that the new non-dimensionalisation reduces the bias towards the electron particle momentum. The multi velocity scaling scheme also finds correct results for the computation of the electric potential where the single velocity scaling scheme does not and the eigenvalues of the multi velocity scaling scheme are more clustered.

Acknowledgments

Je voudrais remercier tout d'abord ma famille; feu mon père qui m'a mit sur cette trajectoire pour devenir ingénieur et ma mère qui a été à mes cotés à chaque moment, sur qui j'ai pu compter en toutes circonstances et en particulier dans les moments difficiles.

Ma petite amie Ondine qui était toujours là pour me réconforter et m'encourager à me faire confiance et persévérer.

J'aimerais aussi remercier les membres du département Aérospatiale et Mécanique et l'équipe ForDGe: Amaury Bilocq, Nicolas Corthouts, Adrien Crovato, Giuseppe Gangemi et Nayan Levaux pour leur patience et disponibilité pour répondre à mes questions et m'aider dans la rédaction de mon manuscrit.

Enfin je voudrais remercier mon promoteur Koen Hillewaert pour sa guidance dans la réalisation de ce travail et pour tout ce qu'il m'a apprit.

I would like to thank first and foremost my family: my late father that put me on this track to become an engineer and my mother whom was besides me every step of the way, on whom I could always rely on and especially through the hard times.

My girlfriend Ondine whom was always present to comfort me and cheer me on to keep going.

I would also like to thank the members of the Aerospace and Mechanics department and the ForDGe team: Amaury Bilocq, Nicolas Corthouts, Adrien Crovato, Giuseppe Gangemi and Nayan Levaux for their patience and availability to answer my questions and help with the writing of my manuscript.

Lastly, I would like to thank my supervisor Koen Hillewaert for his guidance in this endeavor and for everything he has taught me.

Contents

Symbols

Symbol	Name	Symbol	Name
	Plasma Physics		
n_α	number density of species α	v_α	velocity of species α
$S_\alpha^{(m)}$	source term of the variable m of species α	p_α	pressure of species α
m_α	mass of species α	e_α	energy per particle of species α
h_α	enthalpy per particle of species α	q_α	heat exchange rate of species α
Q_α	electrical charge of a particle of species α	V	electrical potential
ϵ_0	permittivity	$\mathbf{E}$	electrical field
$\rho_\pm$	number density of particle with $\pm$ charge	F_e	electrical force
	Discontinuous Galerkin		
$\mathbf{u}$	vector of variables	$\mathbf{F}$	fluxes
ϕ	shape function	Ω	volume of the domain
ϵ	discretized volume of the domain	Ω_e	volume of an element
I	interface surface	f	set of faces of an element
$\mathbf{n}$	normal to the surface of an element	γ^e	interface fluxes of element e
$\mathbf{M}$	mass matrix	$\mathbf{L}$	residual matrix
ξ	parametric coordinates	w_q	quadrature weight
h	time step	$\mathbf{k}$	weighted residual matrix
c_i	time step proportion of Runge-Kutta stage	a_ij	weight of stage j residual for computation of $\mathbf{U}_i$
b_i	Runge-Kutta stage recombination weight	Δt	time step
$\mathbf{U}_i$	stage values of $\mathbf{u}$	$\mathbf{s}$	starter vector for stage value computation
$\Delta\ \mathbf{u}$	difference between two stages	$\mathbf{J}$	Jacobian matrix

Non-dimensionalisation

L_0	length scale	t_0	time scale
κ	heat conductivity	$\mathbf{q}$	vector of corrective factor for time scaling
γ	heat capacity ratio	ρ	density
E	energy density		

Table 1: Symbols

Introduction

Numerical simulation of plasmas is becoming ever more important in a variety of fields and in particular in aerospace. This means that there is a need for a reliable tool to model plasmas. Some applications that are already in use are ablative shielding and electric propulsion. Both these domains require the ability to simulate certain setups and machines to reduce the cost of research and development. This works walks in the steps of the ones who came before in implementing plasma physics in the ForDGe software [3] [10] [9].

The ForDGe software is not the only tool that aims to model plasmas but it is suited to it and it will be a significant upside when it is complete. The goal is to be able to model systems such as Hall effect thrusters. ForDGe uses a discontinuous Galerkin scheme which has high order precision capabilities, allows for complex geometries and is very robust [11] [5]. Current solvers are limited to low order, low dimensional, steady state simulations. Those restrictions make them unfit for simulations of electric thrusters such as Hall effect thrusters [1]. Direct Numerical Simulations or Large Eddy Simulations are necessary to explore and explain certain phenoma that are currently not well understood.

This work is about improving the conditioning of acoustic systems and source terms, specifically the electric potential source term, in plasma. It implies the definition of a new non-dimensionalisation scheme and the integration of a new physic in the ForDGe software. The implementation of electric potential computation had to be taken into account when the new scaling scheme was decided.

Currently ForDGe uses a single velocity scaling scheme for all species of the plasma, specifically in the definition of the scale for the momentum variables. This is to maintain a common time scale across species but results in an unbalanced weight for the different species in the discretised equations. Indeed the particle momentum density of electrons is much larger than that of atoms and ions. Also, mass dnesity is very unbalanced between species while particle density is comparable. ForDGe uses particle momentum density because the number of particles per unit volume (or number density) is more pertinent than the mass density. The chemical reactions and electrical quantities are dependent on the number of particles rather than their mass.

To solve this problem it is proposed to use a species dependent velocity scaling. This re-

sults in a time scaling that is also species dependent. It then becomes paramount to account for differing time scales between equations of the system. To that end explicit and implicit time integration schemes must be revised to accept changes to the time scales.

To measure the effectiveness of the change, the non-dimensionalised variables are compared to check if they are in the same range and order of magnitude. This will indicate that their residual will be comparable and no variable will dominate when calculating the convergence.

The second measure is the convergence rate. Among the algorithms used to solve implicit systems is GMRes. Solving schemes based on Krylov subspaces are susceptible to the eigenvalues of the system they solve. A harmonized scaling scheme will provide more clustered eigenvalues and in turn higher convergence rate.

In addition to the new scaling scheme a new physic will be added, the computation of the electric potential. This is a step towards a complete multifluid modeling of non-neutral plasma and requires adequate scaling as much as the other variables. To check the correct implementation of the electric potential computation it must be analytically derived. This is possible only region by region but will provide the framework for verifying the results.

All in all this work aims to achieve an improvement in the modeling of plasma within the ForDGe software. Both in reworking its scaling and adding new physics. A framework for verification of the results has been put in place and objectives are clear. If achieved the work can be continued by adding the missing physics such as chemistry and electrical forces.

Part I

Theoretical Basis

Chapter 1

Plasma Physics

In this section the different models used to model plasmas will be discussed. This entails the basic properties from gas-like fluids but also plasma specific physics [2] [6] [12].

1.1 Specificities of Plasmas

There are two things that put plasmas apart from gases in terms of physics simulations. That is the type of chemical reactions they can undergo and their interaction with electromagnetic fields.

Plasmas are ionised gases. Ionization reactions are different from other chemical reactions in that a neutral atom can be ionized by a collision with any other particle. The second unique aspect of ionization is the creation of free electrons. Electrons represent a unique challenge because of the disparity in mass between atoms and electrons.

The second specifity of plasmas comes from the first. Through ionization, charged particles are created and will not always bond to form a neutral fluid. This means that computation of electrical potential and its effect on the different particles is paramount to a plasma simulation.

1.2 Conservation Laws

There are several approaches to describing a fluid system. In this work the approach taken is that of conserved quantities. This uses the 1D Boltzmann equation, Eq.1.1, which describes the temporal evolution of a system, for a particle α and a velocity v described by a distribution function $f_\alpha(r, v, t)$ per species, which determines the probability to find a particle at the location (r,v) in state space:

$$\partial_t f_\alpha + v\ \partial_x(f_\alpha) + \partial_v \left(\frac{F_\alpha}{m_\alpha} f_\alpha \right) = S_\alpha^{coll} \tag{1.1}$$

Where F is the total force applied to the particle, m is its mass and S are the collision terms.

The Euler equations are derived from this by taking the first three moments of the Boltzmann equation with respect to velocity, which is sufficient for describing fluid flow in most applications where viscous effects are negligible[1]. The Euler equations describe, not the velocity distribution in state space but, the temporal evolution of average mass density, momentum density and energy density distributions in space as described in Eq.1.2, 1.3 and 1.4:

$$\partial_t \rho_\alpha + \partial_x(\rho_\alpha v_\alpha) = S_\alpha^{(\rho)} \tag{1.2}$$

$$\partial_t(\rho_\alpha v_\alpha) + \partial_x(\rho_\alpha v_\alpha^2 + p_\alpha) = S_\alpha^{(m)} \tag{1.3}$$

$$\partial_t(\rho_\alpha e_\alpha) + \partial_x(\rho_\alpha v_\alpha h_\alpha) = -\partial_x q_\alpha + S_\alpha^{(e)} \tag{1.4}$$

where p is the pressure, h the enthalpy density and q the heat flux. There are 3 equations because that amount is sufficient to describe a thermodynamic system to the needs of the model using closure relations. The quantities in the Euler equations are not, however, the ones used in this paper. Indeed the density is not the best quantity to measure for this application since the rate of chemical reactions and the total charge are dependent on particle number density n rather than mass. The two quantities are linked as follows:

$$n = \frac{\rho}{m_{0,\alpha}} \tag{1.5}$$

with $m_{0,\alpha}$ the particle mass.

In this case the particle density, particle momentum density and particle energy density, which will be referred to as number density, momentum density and energy density from now on, replace the quantities from the Euler equations. These new quantities are the ones form the Euler equations divided by the particle mass of the concerned species. Since those are applicable to each species the complete system is comprised of 3n equations where n is the number of species. The subscript α indicates the species in Eq.4.1, 4.3, 4.7.

$$\partial_t n_\alpha + \partial_x(n_\alpha v_\alpha) = S_\alpha^{(n)} \tag{1.6}$$

$$\partial_t(n_\alpha v_\alpha) + \partial_x(n_\alpha v_\alpha^2 + \frac{p_\alpha}{m_\alpha}) = S_\alpha^{(m)} \tag{1.7}$$

$$\partial_t(n_\alpha e_\alpha) + \partial_x(n_\alpha v_\alpha h_\alpha) = -\frac{1}{m_\alpha}\partial_x q_\alpha + S_\alpha^{(e)} \tag{1.8}$$

[1]The additional diffusive terms in the Navier-Stokes equations stem from the collision term, which is neglected here.

These were derived by dividing the Euler formulae by the particle mass m_α of each species.

1.3 Electrical Potential

Plasmas have the particularity of being composed of charged particles. Those particles generate an electric field which in turn applies a force on the charged particles. Often plasma application will have external electromagnetic fields that also interact with the plasma.

The electromagnetic equations used in this work are derived from the Maxwell equations Eq.1.9, 1.10, 1.11 and 1.12

$$\nabla \cdot \mathbf{E} = \frac{Q}{\epsilon_0} \tag{1.9}$$

with $\mathbf{E}$ the electric field, ϵ_0 the *permittivity* in vacuum and Q the charge density.

$$\nabla \cdot \mathbf{B} = 0 \tag{1.10}$$

with $\mathbf{B}$ the magnetic field;

$$\nabla \times \mathbf{E} = -\frac{1}{c}\frac{\partial \mathbf{B}}{\partial t} \tag{1.11}$$

with c the speed of light,

$$\nabla \times \mathbf{B} = \frac{1}{c}\left(4\pi \mathbf{I} + \frac{\partial \mathbf{E}}{\partial t}\right) \tag{1.12}$$

with $\mathbf{I}$ the current density. The electric and magnetic field exert the Lorentz force (density) on the particles

$$\mathbf{F} = \pm Q_0(\mathbf{E} + \mathbf{v}_p \times \mathbf{B}) \tag{1.13}$$

whereby the sign depends on the charge of the particle ($+$ for ions, $-$ for electrons) and $\mathbf{v}_p$ is the particle velocity. In case the magnetic field is constant, $\mathbf{E}$ is solenoidal and can be defined in function of the electric potential V:

$$\mathbf{E} = -\nabla V, \tag{1.14}$$

Let's assume we have electrons and singly charged ions, with respective particle densities n_- and n_+. The charge density is then $Q = (n_+ - n_-)Q_0$ with Q_0 the elementary charge, and therefore:

$$\nabla \cdot \mathbf{E} = \frac{(n_+ - n_-)Q_0}{\epsilon_0}, \tag{1.15}$$

Hence:

$$\nabla^2 V = -\frac{(n_+ - n_-)Q_0}{\epsilon_0}, \tag{1.16}$$

which is the Poisson equation that governs the electric potential. The electric potential is in turn used to compute source terms in the momentum and energy equations based on the electric force.

$$F_e = n_\alpha \cdot Q_\alpha \cdot \mathbf{E} = n_\alpha \cdot Q_\alpha \cdot (-\nabla V) \tag{1.17}$$

$$S_\alpha^{m,elec} = n_\alpha \cdot Q_\alpha \cdot (-\nabla V) \tag{1.18}$$

$$S_\alpha^{e,elec} = n_\alpha u_\alpha \cdot Q_\alpha \cdot (-\nabla V) \tag{1.19}$$

1.4 Models

Two models have been used for two test cases. The first model is called the Acoustic model and is strictly advective for the conserved quantities. It is used to check the correct implementation of the separate species and the multi scaling applied to them.

The second is called the collisionless model. This model computes electric potential but not interaction through collision. This means no exchange of momentum or kinetic energy between the species and no chemical reactions.

Both models assume no diffusion terms in the number density, momentum density and energy density equations.

1.4.1 Euler Model

The first model for the first test case consists of the Euler equations, scaled with the inverse of the particle mass of each species as presented before. This model has no diffusion and no source terms making it purely hyperbolic.

The conservation laws of the Euler-Like model are:

$$\partial_t n_\alpha + \partial_x(n_\alpha v_\alpha) = 0 \tag{1.20}$$

$$\partial_t(n_\alpha v_\alpha) + \partial_x(n_\alpha v_\alpha^2 + \frac{p_\alpha}{m_\alpha}) = 0 \tag{1.21}$$

$$\partial_t(n_\alpha e_\alpha) + \partial_x(n_\alpha v_\alpha h_\alpha) = 0 \tag{1.22}$$

1.4.2 Acoustic Model

The model for the second test case will be called the acoustic system with electric potential model. This model has only advection for the three conserved quantities, number density, momentum density and energy density, and no diffusion or source terms. It includes both diffusion and sources for the electric potential. The electric potential is the only equation that is not replicated for each species of the plasma. This results in a model where the electric potential is computed but has no effect on the rest of the system. It was used to verify the propagation of shock waves and the computation of the electric potential.

The conservation laws for the acoustic system with electric potential model are:

$$\partial_t n_\alpha + \partial_x(n_\alpha v_\alpha) = 0 \tag{1.23}$$

$$\partial_t(n_\alpha v_\alpha) + \partial_x(n_\alpha v_\alpha^2 + \frac{p_\alpha}{m_\alpha}) = 0 \tag{1.24}$$

$$\partial_t(n_\alpha e_\alpha) + \partial_x(n_\alpha v_\alpha h_\alpha) = 0 \tag{1.25}$$

$$\partial_x(\partial_x V) = -\frac{(n_+ - n_-)Q_0}{\epsilon} \tag{1.26}$$

1.4.3 Collisionless Model

The collisionless model expands on the acoustic model to include effects of the electric potential on the other variables. This includes source terms for the momentum density and the energy density. Collisionless plamsas are approximations of very low density and low temperature plasmas where collisions are so rare that they can be ignored.

The conservation laws for the collisionless model are:

$$\partial_t n_\alpha + \partial_x(n_\alpha v_\alpha) = 0 \tag{1.27}$$

$$\partial_t(n_\alpha v_\alpha) + \partial_x(n_\alpha v_\alpha^2 + \frac{p_\alpha}{m_\alpha}) = n_\alpha \cdot Q_\alpha \cdot -\nabla V \tag{1.28}$$

$$\partial_t(n_\alpha e_\alpha) + \partial_x(n_\alpha v_\alpha h_\alpha) = n_\alpha u_\alpha \cdot Q_\alpha \cdot -\nabla V \tag{1.29}$$

$$\partial_x(\partial_x V) = -\frac{(n_+ - n_-)Q_0}{\epsilon} \tag{1.30}$$

This model was developed but not yet implemented. It is the next step in the development of a complete plasma physic.

Now that a theoretical basis for plasma physics has been established, the next point of interest is the numerical method, the discontinuous Galerkin method.

Chapter 2

Discontinuous Galerkin Method

In this section the Discontinuous Galerkin Finite Element Method (DG-FEM or DG for short) will be introduced [11]. This method for solving Partial Differential Equations (PDE) combines aspects of Finite Element (FEM) and Finite Volume (FVM) methods. More specifically this will be a description of the implementation of the method in the ForDGe software as presented by Bilocq and Levaux in their lecture "Discontinuous Galerkin Method" (2022) [7].

FEM	**FVM**
Characteristics	
Finite cells, elements	Finite cells, volumes
Continuous between elements	Discontinuous between elements
Solution at interpolation nodes	Cell average solution
Pros	
High Order accuracy	Robust due to numerical conservation
Complex geometry	Complex geometry
Well suited for elliptic problems	Well suited for convective problems
Cons	
Not conservative	Need large stencils to achieve high order
Not well suited for convective problems	Not well suited for elliptic problems

Table 2.1: Comparison of FEM and FVM.

The result of combining the two is a method that is more accurate than the Finite Volume Method and more stable than the Finite Element Method. It is suited for problems with a direction, insures numerical conservation of the equations and achieves high order accuracy without large stencils.

2.1 Principles

The DG is used to solve PDEs, in the context of this report the PDEs to solve are 1D conservation laws described in the previous chapter. A general 1D conservation law can be written as Eq.2.1:

$$\partial_t \mathbf{u}(x,t) + \partial_x \mathbf{F}(\mathbf{u}, \partial_x \mathbf{u}, x, t) = \mathbf{S}(\mathbf{u}, x, t) \; x \in \Omega, t \in \mathbb{R} \tag{2.1}$$

Where $\mathbf{u}$ are the conserved quantities, $\mathbf{F}$ are the fluxes, $\mathbf{S}$ are the source and Ω is the domain.

The domain is meshed and divided in elements such that:

$$\Omega \approx \epsilon = \cup_e \; \Omega_e \tag{2.2}$$

and the boundary of each element e is the union of all the interfaces with neighboring elements such that:

$$\partial\Omega_e = \cup_f \; I_f, \tag{2.3}$$

The solution is interpolated in the Broken Sobolev space $\mathcal{V}^p$ that consists of functions that are regular polynomials of given order p inside each element but not necessarily continuous across element boundaries.

The exact solution is interpolated using a set of basis functions ϕ_i, also called the trial functions:

$$u = \sum_i \phi_i u_i \tag{2.4}$$

The expansion weights u_i are found by requiring that the residual of equations Eq. 2.1 is orthogonal to all functions in $\mathcal{V}$; this is called the Galerkin variational formulation. In practice, this is tested for each function ϕ_i in the basis; since all functions in $\mathcal{V}$ are linear combinations of the ϕ_i, this is sufficient. Integrating over the domain Ω Eq.2.5, the following equation is formally satisfied:

$$\int_\Omega (\partial_t \mathbf{u} - \mathbf{S})\phi \; dV + \int_\Omega \phi \nabla \partial_x \mathbf{F} \quad dV = 0, \; \forall \phi \in \mathcal{V}^p \tag{2.5}$$

After splitting the integral in a sum over all elements, performing integration by parts on each of the elements, and testing for each ϕ_i in the basis for $\mathcal{V}$, we arrive at equation Eq.2.6 :

$$\sum_e \left(\int_{\Omega_e} (\partial_t \mathbf{u} - \mathbf{S}) \phi_i \, dV - \int_{\Omega_e} \mathbf{F} \, \partial_x \phi_i \, dV + \oint_{\partial\Omega_e} \mathbf{F} \, \mathbf{n} \, \phi_i \, dS \right) = 0 \quad \forall \phi_i \tag{2.6}$$

The DGM then proceeds by collecting the fluxes of both elements on the shared interfaces, and replacing the sum with a suitable interface flux γ^f, which is function of the solution and test function on either side, as shown in Eq.2.7:

$$\begin{aligned} \sum_e \oint_{\Omega_e} \mathbf{F} \, \mathbf{n} \, \phi_i \, dS &= \sum_f \oint_{\Omega_f} \mathbf{F} \, \mathbf{n} \, \phi_i \, dS \\ &= \sum_f \oint_{\Omega_f} (\phi_i^+ \mathbf{F}^+ \mathbf{n}^+ + \phi_i^- \mathbf{F}^- \mathbf{n}^-) dS \\ &= \sum_f \oint_{\Omega_f} \gamma^f(u^+, u^-, \phi^+, \phi^-) dS, \end{aligned} \tag{2.7}$$

In practice this would mean a γ^f that is consistent and ensures stability. $\mathbf{F}^\pm$ and $\mathbf{n}^\pm$ are as presented in Fig.5.1:

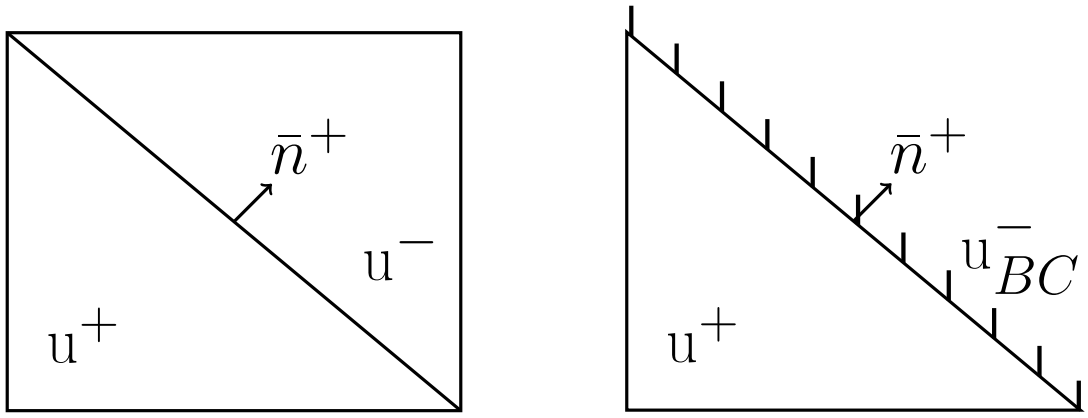

Figure 2.1: Interface flux.

This all comes together in Eq.2.8.

$$\sum_e \int_{\Omega_e} (\partial_t \mathbf{u} - \mathbf{S}) \phi_i \, dV - \sum_e \int_{\Omega_e} \mathbf{F} \, \partial_x \phi_i \, dV + \sum_{f \in \partial\Omega_e} \oint_f \gamma^f \, dS = 0 \tag{2.8}$$

For practical reasons, a set of basis functions ϕ_i^e is chosen which are:

- Polynomial functions of order below or equal to p inside a given element;

- Zero outside of their element;
- Equal to 1 at one interpolation point and zero at the others;
- The sum of all functions is equal to 1 in each element, and by extension over the whole domain

This choice ensures that the equation for test function ϕ_i can be evaluated using a single element for the volume term and only its direct neighbors for the interface, instead of involving an integral over all elements and interfaces over the whole domain.

2.2 Semi-Discrete Form and Residual

The next step is defining the semi-discrete form. The semi-discrete form is in the form of Eq.2.9:

$$\partial_t \mathbf{u}_i^e = \mathbf{M}^{-1}\mathbf{L} \tag{2.9}$$

This form is obtained by using the quadrature rules in Eq.2.10 the index q represents the quadrature point.

$$\int_{-1}^{1} f(\xi)d\xi \approx \sum_{q=0}^{n} w_q f(\xi_q) \tag{2.10}$$

$\mathbf{M}$ is the mass matrix:

$$\mathbf{M}_{ij} = \sum_{q=0}^{n} w_q \phi_i \phi_i \tag{2.11}$$

$\mathbf{L}$ is the residual:

$$\mathbf{L} = \sum_{q=0}^{n} w_q \phi_i^e \mathbf{S} + \sum_{q=0}^{n} w_q \nabla\phi_i^e \mathbf{F} + \sum^{f}\sum_{q=0}^{n} w_q \gamma^e \tag{2.12}$$

2.3 Time Integration

From the discrete form a time integration scheme can be applied. Two such schemes will be tested, both from the Runge-Kutta family. First the "explicit Runge-Kutta of order 4" scheme and second the implicit scheme "Explicit Single Diagonal Implicit Runge Kutta" (ESDIRK) [4].

2.3.1 Runge-Kutta

All schemes from the Runge-Kutta family follow a similar structure: it evaluates a function **u** at successive times steps n. It does so by multiplying a linear combination of the time derivative **k** of **u** by the length of the time step h. This process can take the form of Eq.2.13:

$$\mathbf{u}^{n+1} = \mathbf{u}^n + \frac{h}{\sum b_i} \sum b_i \cdot \mathbf{k}_i \tag{2.13}$$

Which when combined with the semi-discrete form of Eq.2.9 results in Eq.2.14

$$\mathbf{u}^{n+1} = \mathbf{u}^n + \frac{h}{\sum b_i} \sum b_i \cdot \mathbf{M}^{-1}\mathbf{L} \tag{2.14}$$

These methods can be described by what is called a Butcher's tableau which takes the form of Tab.2.2

c_1	a_{11}	a_{12}	a_{13}	a_{14}
c_2	a_{21}	a_{22}	a_{23}	a_{24}
c_3	a_{31}	a_{32}	a_{33}	a_{34}
c_4	a_{41}	a_{42}	a_{43}	a_{44}
	b_1	b_2	b_3	b_4

Table 2.2: Butcher's Tableau of a 4 stage Runge-Kutta scheme

Where the c and a values represent the parameters with which the stage values $\mathbf{U}_i^n$ are computed according to the Eq.2.15

$$\mathbf{k}_i = \mathbf{f}(t_0 + c_i \cdot \Delta t, \mathbf{u}_0 + \Delta t \sum_{j=1}^{i} a_{ij}(\mathbf{M}^{-1}\mathbf{L})_j) \tag{2.15}$$

Explicit Runge-Kutta schemes will have only 0 on and above the diagonal, not requiring the Residual of the stage currently being computed to determine it.

Implicit Runge-Kutta schemes can have non-zero values on the diagonal and above, requiring a linear solver to compute each stage. In practice these schemes have non-zero values on the diagonal but not above.

$$\mathbf{U}_i = \mathbf{u}^n + \Delta t \sum_{j=0}^{i} a_{ij} (\mathbf{M}^{-1}\mathbf{L})_j \tag{2.16}$$

Is solved iteratively until Eq.2.17

$$\mathbf{U}_i = \mathbf{s}_i + \Delta t a_{ii} (\mathbf{M}^{-1}\mathbf{L})_j (\mathbf{U}_i) \tag{2.17}$$

Where the starter vector $\mathbf{s}$ is:

$$\mathbf{s}_i = \mathbf{u}^n + \Delta t \sum_{j=0}^{i-1} a_{ij} (\mathbf{M}^{-1}\mathbf{L})_j \tag{2.18}$$

In the case of the electric potential equation, which is non-temporal, this scheme is not applicable since the value of the electric potential at a given time step is not dependent on its value at any previous or future time step. This required the deactivation of the inertial term for the electric potential equation.

The Butcher's tableau of the two considered methods are available in the Appendix A

2.3.2 Solvers

For the implicit stages of the time schemes a solver is required. The solver in this case is the Newton-Raphson algorithm which itself uses the Generalised Minimum Residual (GMRes) iterative method for solving the associated linear problem. The Newton-Raphson algorithm is a root finding method applied to the expression of the difference between the current stage and the initial state $\Delta \mathbf{u}_i$.

$$\frac{\mathbf{U}_{i+1} - \mathbf{U}_i}{\Delta t} = \frac{\Delta \mathbf{u}_i}{\Delta t} = \sum_{j=0}^{i} a_{ij} (\mathbf{M}^{-1}\mathbf{L})_j \tag{2.19}$$

The residual is then split into its explicit and implicit parts, expressing the implicit part as a function of the Jacobian.

$$\frac{\Delta \mathbf{u}_i}{\Delta t} = a_{ii} (\mathbf{M}^{-1}\mathbf{L})_i + \sum_{j=1}^{i-1} a_{ij} (\mathbf{M}^{-1}\mathbf{L})_j \tag{2.20}$$

$$(\mathbf{M}^{-1}\mathbf{L})_i = (\mathbf{M}^{-1}\mathbf{L})_{i-1} + \mathbf{M}^{-1}\mathbf{J}\Delta \mathbf{u}_i \tag{2.21}$$

Combining Eq.2.20 and 2.21 the following system is obtained:

$$\left(\frac{\mathbf{I}}{a_{ii}\Delta t} - \mathbf{M}^{-1}\mathbf{J}\right)\Delta\mathbf{u}_i = (\mathbf{M}^{-1}\mathbf{L})_{i-1} + \frac{1}{a_{ii}}\sum_{j=1}^{i-1} a_{ij}(\mathbf{M}^{-1}\mathbf{L})_j \tag{2.22}$$

Which is of the form:

$$\mathbf{A}x = \mathbf{b} \tag{2.23}$$

And can thus be solved using the GMRes method.

In the case of the electric potential which has no inertial term the equations are slightly different.

$$0 = a_{ii}(\mathbf{M}^{-1}\mathbf{L})_i \tag{2.24}$$

Which, by the same process, becomes:

$$\left(-\mathbf{M}^{-1}\mathbf{J}\right)\Delta\mathbf{u}_i = (\mathbf{M}^{-1}\mathbf{L})_{i-1} \tag{2.25}$$

The physics having been translated into a numerical model, the next step is to define the problem to be solved. To ensure that the problem is solved to satisfaction it is important to consider how it is presented. It entails the choice a scaling of the variables also called conditioning.

Part II

Conditioning

Chapter 3

Motivation

Working towards the good conditioning of a system can have multiple reasons. In this case the motivation for the conditioning of the system is to increase precision and convergence rate. This is achieved through the use of a non-dimensionalisation that is species dependent. The details of this non-dimensionalisation will be discussed in chapter 4.

Using an non-dimensionalisation that is not species dependent results in a velocity scaling that is not appropriate for one of two groups of species, either the electrons or the heavy species, since the electrons will move at a speed about 270 times faster than the heavies in the case of an argon3 plasma.

This is then reflected in the variables of the problem. Indeed both momentum and energy scaling are dependent on the velocity and the residuals even more so.

3.1 Precision

The variable affected by the multi velocity scaling is the momentum of the electrons. Indeed the number density scaling remains singular among the species and the difference in mass between ions and atoms is so small that the scaling difference can be ignored for the purposes of this work. The electric potential is not dependent on the velocity and thus is not affected.

With the multi velocity scaling, each species is scaled according to its own parameters, meaning that they will have similar profiles, the only difference being time. Considering this, it becomes obvious that the non-dimensionalised electron momentum would have values many orders of magnitude greater than that of other variables. The momentum is the only variable that uses the velocity scaling in its computation.

The species dependent velocity scaling v_0 is defined

$$v_0 = \sqrt{\frac{k_B T_0}{m_{0,\alpha}}}, \tag{3.1}$$

and is used to compute the momentum scales:

$$momentum_{0,\alpha} = n_0 v_{0,\alpha}, \tag{3.2}$$

It is then possible to show the difference in scales:

Scaled Variable	Single Velocity Scaling	Multi Velocity Scaling
Number Density [-/m^3]	1.65E+23	1.65E+23
Momentum Density [-/s m^2]	4.13E+25	1.11E+28
Energy Density [-/s^2 m]	7.50E+32	7.50E+32

Table 3.1: Comparison of the scales used to non-dimensionalise the number density, momentum density and energy density of electrons for single velocity and multi velocity scaling schemes.

This disparity in scales shows that since the multi velocity scaling has balanced varaibles, the single velocity scaling has very unbalanced variables.

This imbalance is significant because of the way that convergence is computed by both the Newton-Raphson and GMRes algorithms. Indeed the method used for convergence relies on the minimisation of the residual as measured by the method of least squares and L2 norm.

In both these methods if one or more variable greatly exceeds the others, only that variable will direct the convergence of the algorithm.

3.2 Convergence Rate

3.2.1 Principles

In a similar way the convergence of the GMRes algorithm is impacted by the different scalings. The convergence rate of the GMRes algorithm is dependent on the eigenvalues of the matrix **A** in Eq.2.23. Clustered values mean a faster convergence and faster convergence allows for a higher threshold for convergence in the same amount of time. That is because clusterd values mean a condition number close to 1 and thus a matrix more easily inverted. This added precision is compounded on each Newton iteration into a faster again convergence.

The exact impact of the scaling on those eigenvalues is complex because having a species dependent velocity scaling will impose a different time scaling too. Thus the new non-dimensionalisation will change both the Jacobian and the inertial term that depends on the time step. Before analyzing those effects, it is thus pertinent to define the change in velocity scaling.

3.2.2 Metrics

When determining whether the multi velocity scaling is favorable the criteria that will be used is the clustering of the eigenvalues of the expanded Jacobian matrix.

According to Salgado and Wise [15], the convergence rate of the GMRes algorithm is dependent on the geometry of the the ellipse $\mathcal{E}$ that holds all of the eigenvalues of the expanded Jacobian. This ellipse is defined as having a center c, excentricity d and semi-major axis a. Let us assume a problem of the form:

$$\mathbf{A}x = \mathbf{b} \tag{3.3}$$

where the expanded Jacobian $\mathbf{A} \in \mathbb{C}^{nxn}$ is nonsingular and diagonalizable such that $\mathbf{A} = \mathbf{V}\Lambda\mathbf{V}^{-1}$ and $\mathbf{b} \in \mathbb{C}^n_*$, where Λ is a diagonal matrix with the eigenvalues of $\mathbf{A}$ on the diagonal.

The clustering is important because the convergence rate can be expressed using the parameters of the ellipse as follows:

$$||\mathbf{L}_k||_2 \leq \kappa_2(\mathbf{V})\frac{C_k(\frac{a}{d})}{|C_k(\frac{c}{d})|}||\mathbf{L}_0||_2, \tag{3.4}$$

where $0 \notin \mathcal{E} \subset \mathbb{C}$, the starting x is arbitrary, κ_2 is the condition number and $\mathbf{L}_k = \mathbf{b} - \mathbf{A}x_k$. C is defined as:

$$C_k(z) = (z + \sqrt{z^2 - 1})^k + (z + \sqrt{z^2 - 1})^{1/k} \tag{3.5}$$

which shows that the semi-major axis must be minimized while the center must be placed as far as possible.

With the objectives and metrics of success laid out the implementation can begin, this starts with the definition of the new non-dimensionalisation scheme.

Chapter 4

Non-dimensionalization

The first iteration of the software used a single reference velocity, that of the neutrals, atoms, in order to maintain a single time sale. It has been found to be too much of a compromise. This has led to the idea of implementing a variable non-dimensionalization.

The variable time scale has an impact on the time integration which will be discussed in section 4.2.

The non-dimensionalization is driven by 2 factors:

First, it is desirable to express the variables of the problem in similar scales (typically close to 1) because then no variable is more important than another in the computation of convergence and neither is a species more important than another. This is the reason for species dependent non-dimensionalization.

Second it is desirable to not introduce coefficients in the conservation law. That is why the species dependent velocity scale implies a species dependent time scale. This strategy was then implemented for diffusion and source terms as well.

4.1 Species Dependent Velocity Scaling

As the title indicates, this is an non-dimensionalization that uses a species dependent velocity reference. This section expresses the conservation equations under the new non-dimensionalization and then explores its effect on the resolution of the system of PDEs.

4.1.1 Equations

First the conservation equations are re-expressed with reference scales (0 subscript) and non-dimensionalized values ($'$ superscript). The aim was to have no coefficient in front of the convection term.

The number density equation

$$\partial_t n_\alpha + \partial_x (n_\alpha v_\alpha) = S_\alpha^{(n)} \tag{4.1}$$

Becomes:

$$\begin{aligned} \frac{n_{0,\alpha}}{t_{0,\alpha}} \partial_{t'} n'_\alpha + \frac{n_{0,\alpha} v_{0,\alpha}}{L_0} \partial_{x'} (n'_\alpha v'_\alpha) &= S_{0,\alpha}^{(n)} S_\alpha'^{(n)} \\ \frac{L_0}{v_{0,\alpha} t_{0,\alpha}} \partial_{t'} n'_\alpha + \partial_{x'} (n'_\alpha v'_\alpha) &= \frac{L_0 S_{0,\alpha}^{(n)}}{n_{0,\alpha} v_{0,\alpha}} S_\alpha'^{(n)} \end{aligned} \tag{4.2}$$

The momentum equation

$$\partial_t (n_\alpha v_\alpha) + \partial_x (n_\alpha v_\alpha^2 + \frac{p_\alpha}{m_\alpha}) = S_\alpha^{(m)} \tag{4.3}$$

Becomes:

$$\begin{aligned} \frac{n_{0,\alpha} v_{0,\alpha}}{t_{0,\alpha}} \partial_{t'} (n'_\alpha v'_\alpha) + \frac{n_{0,\alpha} v_{0,\alpha}^2}{L_0} \partial_{x'} (n'_\alpha v'^2_\alpha + \frac{p'_\alpha}{m'_\alpha}) &= S_{0,\alpha}^{(m)} S_\alpha'^{(m)} \\ \frac{L_0}{v_{0,\alpha} t_{0,\alpha}} \partial_{t'} (n'_\alpha v'_\alpha) + \partial_{x'} (n'_\alpha v'^2_\alpha + \frac{p'_\alpha}{m'_\alpha}) &= \frac{L_0 S_{0,\alpha}^{(m)}}{n_{0,\alpha} v_{0,\alpha}^2} S_\alpha'^{(m)} \end{aligned} \tag{4.4}$$

With:

$$p_{0,\alpha} = n_{0,\alpha} m_{0,\alpha} v_{0,\alpha}^2 \tag{4.5}$$

The energy equation

$$\partial_t (n_\alpha e_\alpha) + \partial_x (n_\alpha v_\alpha h_\alpha) = -\frac{1}{m_\alpha} \partial_x q_\alpha + S_\alpha^{(e)} \tag{4.6}$$

Becomes:

$$\frac{n_{0,\alpha}e_{0,\alpha}}{t_{0,\alpha}}\partial_{t'}(n'_\alpha e'_\alpha)+\frac{n_{0,\alpha}v_{0,\alpha}e_{0,\alpha}}{L_0}\partial_{x'}(n'_\alpha v'_\alpha h'_\alpha)=\frac{\kappa_{0,\alpha}T_{0,\alpha}}{m_{0,\alpha}L_0^2}\frac{1}{m'_\alpha}\partial_{x'}\kappa'_\alpha\partial_{x'}T'_\alpha+S^{(e)}_{0,\alpha}S'^{(e)}_\alpha$$

$$\frac{L_0}{v_{0,\alpha}t_{0,\alpha}}\partial_{t'}(n'_\alpha e'_\alpha)+\partial_{x'}(n'_\alpha v'_\alpha h'_\alpha)=\frac{\kappa_{0,\alpha}T_0}{n_{0,\alpha}v_{0,\alpha}e_{0,\alpha}m_{0,\alpha}L_0}\frac{1}{m'_\alpha}\partial_{x'}\kappa'_\alpha\partial_{x'}T'_\alpha+\frac{S^{(e)}_{0,\alpha}L_0}{n_{0,\alpha}v_{0,\alpha}e_{0,\alpha}}S'^{(e)}_\alpha \tag{4.7}$$

Where:

$$q_\alpha=-\kappa_\alpha\partial_x T_\alpha \tag{4.8}$$

The Electric Potential Equation

$$\partial_x(\partial_x V)=-\frac{(n_+-n_-)Q_0}{\epsilon} \tag{4.9}$$

Becomes:

$$\frac{V_0}{L_0^2}\partial_{x'}(\partial_{x'}V')=-n_{0,\alpha}\frac{(n'_+-n'_-)Q_0}{\epsilon} \tag{4.10}$$

$$\partial_{x'}(\partial_{x'}V')=-\frac{n_{0,\alpha}L_0^2}{V_0}\frac{(n'_+-n'_-)Q_0}{\epsilon} \tag{4.11}$$

Which results in the following scales:

Scale	Parameter	Expression	Description
L_0	Length	1	For Simplicity
$m_{0,\alpha}$	Mass	m_α	Mass of the α species' particle
$n_{0,\alpha}$	Particle Density	TBD	Relevant particle density
$v_{0,\alpha}$	Velocity	$\sqrt{\frac{k_B \cdot T_{0,\alpha}}{m_{0,\alpha}}}$	Particle velocity to have Euler number = 1
$T_{0,\alpha}$	Temperature	$\frac{v_{0,\alpha}^2 m_{0\alpha}}{k_B}$	Follows from velocity
$p_{0,\alpha}$	Pressure	$n_{0,\alpha} \cdot m_{0,\alpha} \cdot v_{0,\alpha}^2$	Follows from temperature
$E_{0,\alpha}$	Energy per particle	$v_{0,\alpha}^2 = \frac{k_B \cdot T_{0,\alpha}}{m_{0,\alpha}}$	Follows from pressure
t_0	Time	$v_{0,\alpha} \cdot L_0$	so that $\frac{L_0}{v_{0,\alpha} t_{0,\alpha}} = 1$
$S_{0,\alpha}$	Source	TBD	Dependent on model used

In practice it is the choice of reference temperature, particle mass and particle density that will determine the other scales. Mainly because the velocity, pressure and energy follow from it but also because it will be heavily used in the source scale. This scheme allows for different reference temperatures but it is not expected to be necessary.

4.2 Impact on the implementation

In order to not have a coefficient in front of the time partial derivative it is posited that:

$$t_{0,\alpha} = \frac{L_0}{v_{0,\alpha}} \tag{4.12}$$

This means that a different time scale is used for each species. In turn this has an impact on the computation of the residual. More specifically, in the Runge-Kutta time integrator, a correction must be introduced.

4.2.1 General Time Derivative Scaling

The new scaling offers a better convergence control but it means that the conservation equations are of the form:

$$\begin{bmatrix} \partial_{t_e} \mathbf{u}_e \\ \partial_{t_i} \mathbf{u}_i \\ \partial_{t_n} \mathbf{u}_n \end{bmatrix} = \begin{bmatrix} Res(\mathbf{u}_e) \\ Res(\mathbf{u}_i) \\ Res(\mathbf{u}_n) \end{bmatrix} \tag{4.13}$$

Which clearly shows the issue. While the physical time step remains the same, the residuals are computed as though each species evolves at its own time. It becomes even more clear when the relation between the time derivatives is shown in Eq.4.14 and 4.15

$$\frac{\partial}{\partial_{t_{0,\alpha}}} = \frac{\partial}{\partial_{t_{0,\beta}}} \frac{\partial_{t_{0,\beta}}}{\partial_{t_{0,\alpha}}} = \frac{v_{0,\beta}}{v_{0,\alpha}} \frac{\partial}{\partial_{t_{0,\beta}}} = q_\beta \frac{\partial}{\partial_{t_{0,\beta}}} \tag{4.14}$$

Because:

$$t_{0,\beta} = v_{0,\beta} L_0 = \frac{v_{0,\beta}}{v_{0,\alpha}} v_{0,\alpha} L_0 = \frac{v_{0,\beta}}{v_{0,\alpha}} t_{0,\alpha} \tag{4.15}$$

To arrive at a uniform time derivation some equations must be multiplied by a certain factor q_α to make the right time derivative appear.

$$\begin{bmatrix} \partial_{t_\alpha} \mathbf{u}_e \\ \partial_{t_\alpha} \mathbf{u}_i \\ \partial_{t_\alpha} \mathbf{u}_n \end{bmatrix} = \begin{bmatrix} q_e \cdot Res(\mathbf{u}_e) \\ q_i \cdot Res(\mathbf{u}_i) \\ q_n \cdot Res(\mathbf{u}_n) \end{bmatrix} \tag{4.16}$$

Or

$$\partial_{t_\alpha} \mathbf{u}_\alpha = q_\alpha \cdot Res(\mathbf{u}_\alpha) \tag{4.17}$$

4.2.2 Impact on the Runge Kutta Schemes

Eq.4.17 is then plugged into the Runge-Kutta non-dimensionalisation which gives:

$$\frac{\Delta \mathbf{u}_i}{\Delta t} = \mathbf{q}\ a_{ii} (\mathbf{M}^{-1}\mathbf{L})_i + \mathbf{q} \sum_{j=1}^{i-1} a_{ij} (\mathbf{M}^{-1}\mathbf{L})_j \tag{4.18}$$

Which can be developed like previously into:

$$\left(\frac{\mathbf{q}^{-1}\mathbf{I}}{a_{ii}\Delta t} - \mathbf{M}^{-1}\mathbf{J}\right)\Delta\mathbf{u}_i = (\mathbf{M}^{-1}\mathbf{L})_{i-1} + \frac{1}{a_{ii}}\sum_{j=1}^{i-1} a_{ij}(\mathbf{M}^{-1}\mathbf{L})_j \tag{4.19}$$

4.3 Impact on the convergence of GMRes

The convergence of the GMRes scheme when solving with the implicit Runge-Kutta scheme is dependent on the eigenvalues of the matrix:

$$\left(\frac{\mathbf{q}^{-1}\mathbf{I}}{a_{ii}\Delta t} - \mathbf{M}^{-1}\mathbf{J}\right) \tag{4.20}$$

Which is calculated:

$$\det\left|\left(\frac{\mathbf{q}^{-1}\mathbf{I}}{a_{ii}\Delta t} - \mathbf{M}^{-1}\mathbf{J}\right) - \lambda\mathbf{I}\right| \tag{4.21}$$

Let $\bar{\lambda}$ be the eigenvalues of the mass matrix and Jacobian product alone then:

$$\lambda\mathbf{I} = \left(\bar{\lambda}\mathbf{I} + \frac{\mathbf{q}^{-1}\mathbf{I}}{a_{ii}\Delta t}\right) \tag{4.22}$$

In a non scaled system the $\bar{\lambda}$ are in velocity units. This means that in the single velocity scaling those values are ≈ 271 times larger for electrons than argon atoms. In the multi velocity scaling this is remedied by the species dependent scales. The time scales are also different but this change is wholly countered by the value of q for the heavy species.

The conditioning done, the simulation can be done. There are 2 test cases used to show the impact of the multi velocity scaling, each showing a different aspect of the change.

Part III

Results

Chapter 5

Step Propagation

The test cases used in this work are based on a very common test case. They are the propagation of a simple step in number density. This is also known as the sod shock tube test. This is a famous test case because it illustrates several mechanics of the model and has well understood results. Those results are less understood when it comes to the electric potential and the propagation of two fluids with very different properties.

5.1 Test Case

The parameters of this test case are rather simple with the caveat that since this is a plasma there are 3 distinct fluids. All the fluids are subject to the same initial conditions (IC) and boundary conditions (BC). Those conditions are:

General Conditions

- The test case is 1D
- The domain is 1m wide
- Only advection except for the electric potential

Initial Conditions

- The fluid has a homogeneous temperature of 300 K
- The fluid has a homogeneous velocity of 0 m/s
- The fluid has 2 homogeneous zones of density separated in the middle of N0 and N0/2
- The electric potential starts with a value of zero at the left border

- The electric potential first derivative is zero on the right border

Boundary Conditions

- The fluid cannot cross the borders of the domain
- No heat is exchanged at the borders of the domain

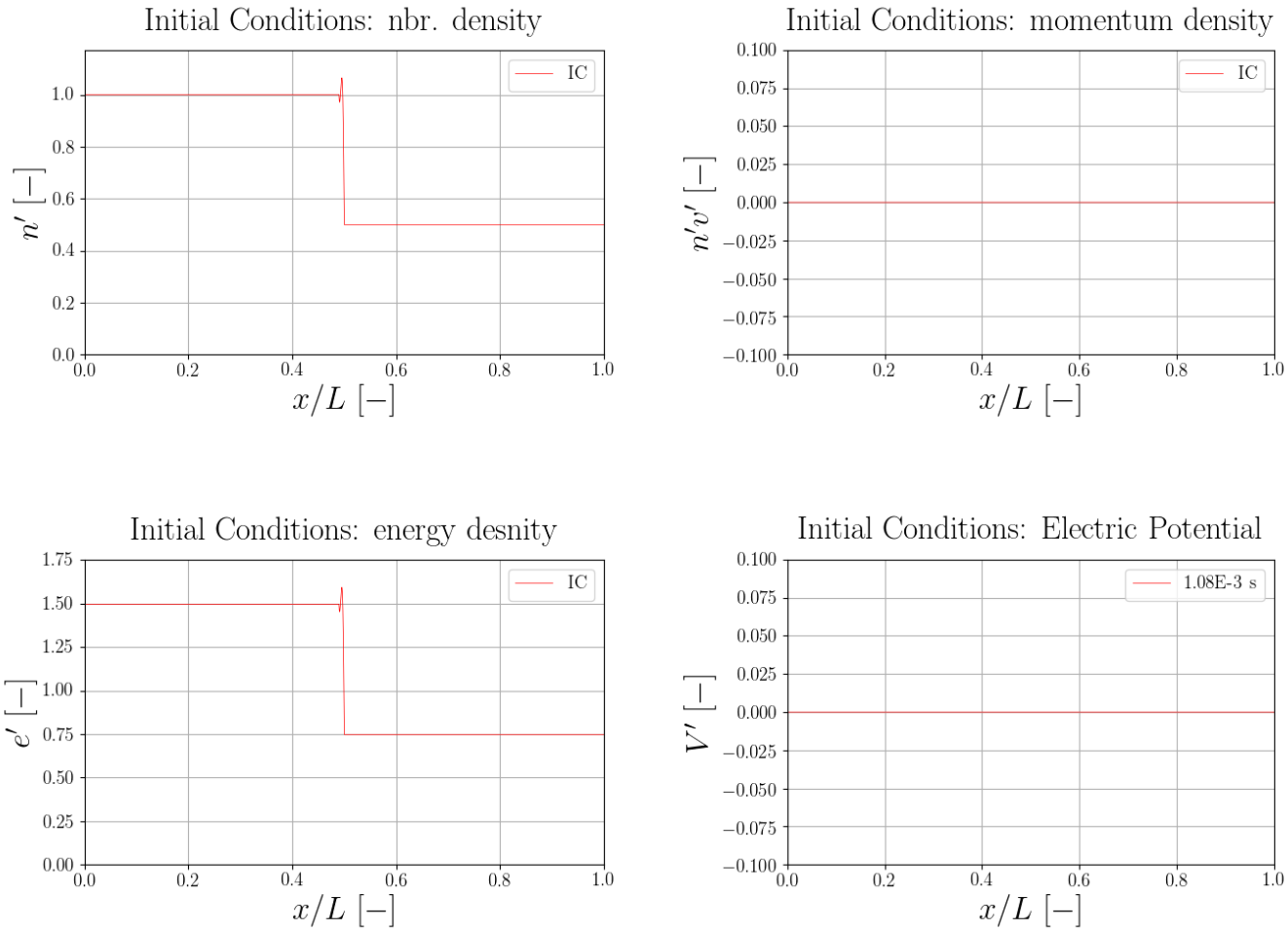

Figure 5.1: Initial Conditions of the test cases.

5.2 Analytical Solution

This test case is a form of Riemann problem for modified Euler equations for 3 systems of different fluids. The solution of the Riemann problem for the Euler equations is applicable

by substituting the mass by the number of particles since those quantities are proportional.

The solution presented here comes from Randall J. Leveque's "Numerical Methods for Conservations Laws" [14]. This solution uses the principles of shock propagation and the variables are the density ρ, momentum density ρv and energy density E.

A first analysis of the problem takes the form of computing the Jacobian and solving the eigenvalue problem.

$$\begin{bmatrix} 0 & 1 & 0 \\ \frac{1}{2}(\gamma-3)v^2 & (3-\gamma)v & (\gamma-1) \\ \frac{1}{2}(\gamma-1)v^3 - v(E+p)/\rho & (E+p)/\rho - (\gamma-1)v^2 & \gamma v \end{bmatrix} \tag{5.1}$$

Where γ is the heat capacity ratio and p is the pressure. From this the three eigenvalues

$$\lambda_1 = v - c, \tag{5.2}$$

$$\lambda_2 = v, \tag{5.3}$$

$$\lambda_3 = v + c, \tag{5.4}$$

are derived. With

$$c = \sqrt{\frac{\gamma p}{\rho}}, \tag{5.5}$$

the speed of sound.

5.2.1 Shock Propagation Prediction

The second charateristic field of eigenvectors is linearly degenerate meaning it is a contact discontinuity. This can be checked seeing that

$$r_2(u) = \begin{bmatrix} 1 \\ v \\ \frac{1}{2}v^2 \end{bmatrix}, \tag{5.6}$$

is an eigenvector of the Jacobian with eigenvalue $\lambda_2(\mathrm{u}) = v = (\rho\ v)\ /\ \rho$ since

$$\nabla\lambda_2(u) = \begin{bmatrix} -\frac{v}{\rho} \\ \frac{1}{\rho} \\ 0 \end{bmatrix}, \tag{5.7}$$

resulting in

$$\nabla\lambda_2 \cdot r_2 \equiv 0, \tag{5.8}$$

meaning that it can neither be a rarefaction wave or a shock.

The other two are not degenerate but that will not be demonstrated here. Observing the speeds of sound on each side of the remaining characteristics it can be seen that the first, on the left in this case, is a rarefaction wave and the third, on the right, is a shock.

The system of discontinuities can then be represented with:

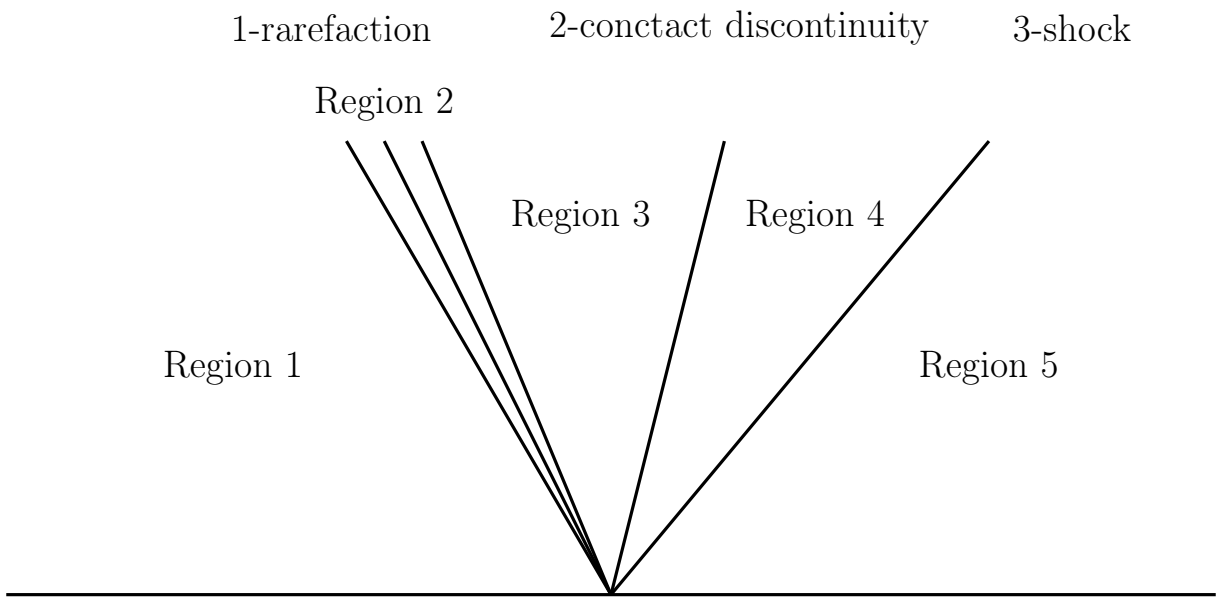

Figure 5.2: System of Discontinuities

It is then possible to compute the states around each discontinuity. This requires an iterative solving but results in the following density distribution after a time 4E-6 s for electrons.

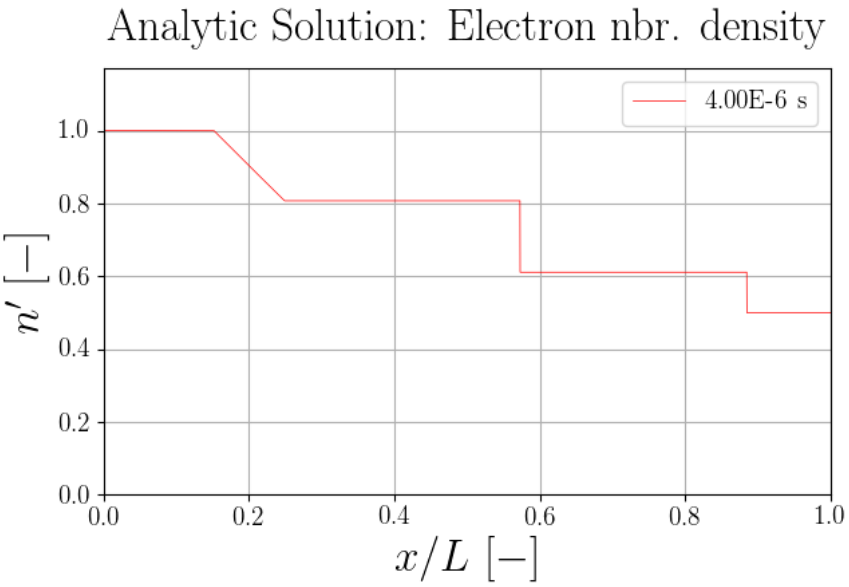

Figure 5.3: Analytical prediction of the Number Density distribution at 4E-6s of the electrons.

And the distribution of density of the heavy species after 1.08E-3 s is the same.

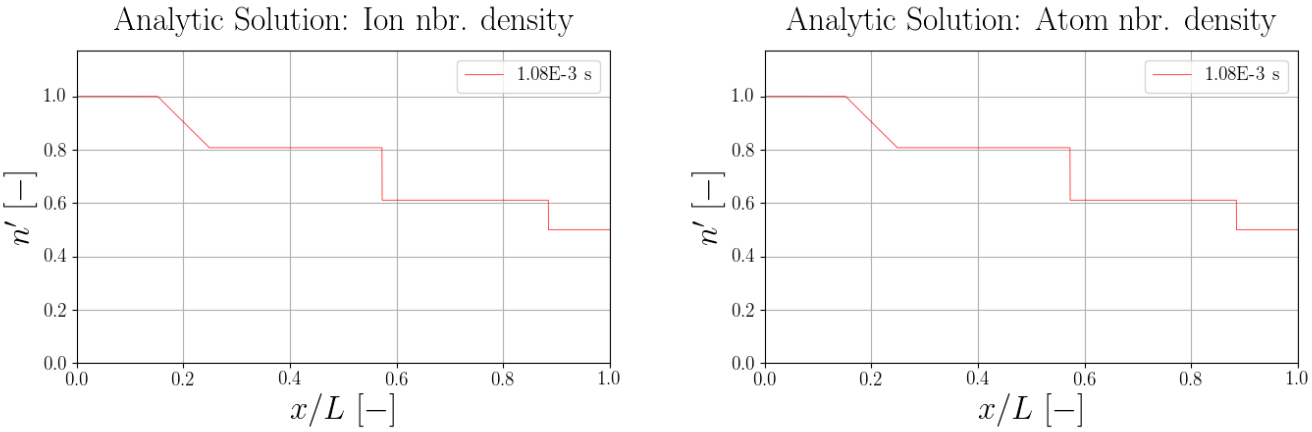

Figure 5.4: Analytical prediction of the Number Density distribution at 1.08E-3s of the heavy species.

5.2.2 Electric Potential Prediction

Predicting the electric potential analytically requires the solving of 6 PDEs, one in each region of the density distribution and two in the third region as the number density of ions changes while the electron number density remains the same. Each PDE also requires IC that are dependent on the previous solution.

The IC placed on the electric potential in the test case are on opposite sides of the domain. On the left border the electric potential is set to zero and on the other the first derivative is set to zero. However it is possible to deduce the first derivative of the electric potential on the left side from the IC.

Indeed since the PDE used is

$$\partial_{xx} V = \frac{(q_+ - q_-)e_0}{\epsilon_0}, \tag{5.9}$$

and since the domain contains, per the IC, an equal amount of positively and negatively charged particles, the integral over the domain of those amounts equals zero. This means that the integral over the domain of the second derivative of the electric potential is also equal to zero. This means that the first derivative at the right border is equal to the derivative at the left border.

It then becomes possible to solve, region by region, the PDEs that determine the electric potential. The first and fifth regions have the same amount of positively and negatively charged particle and thus there is no change to the potential. This leaves 4 PDEs to solve.

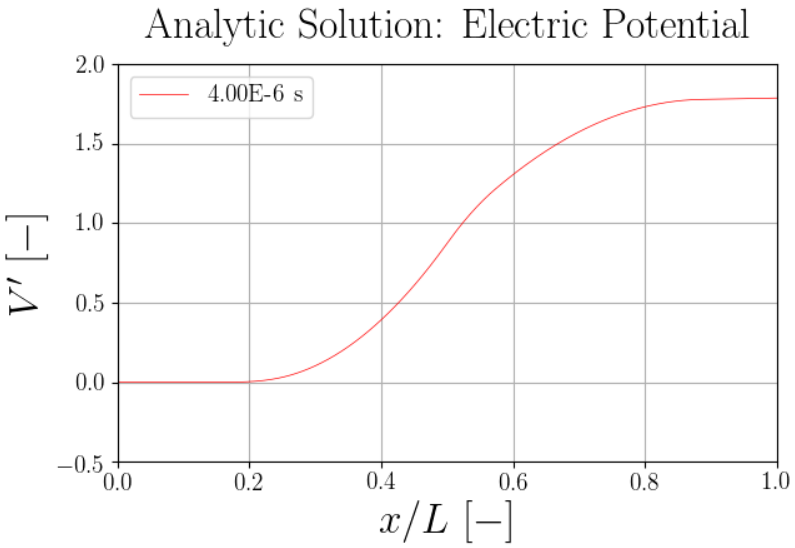

Figure 5.5: Analytical prediction of the electric potential at 4E-6s.

The analytical solution will be paramount in the verification of the results; it would be pointless to compare erroneous solutions. The test cases can now be studied knowing the results are correct.

Chapter 6

Sod Shock Tube with Euler-Like Equations

The Euler-Like test case is called so because of the equations used in the system. Rather than being based on mass per unit volume they are based on number of particles per unit volume which yields almost identical results based on the non-dimensionalisation used.

6.1 Validation of the Results

Before studying the impact of the new non-dimensionalisation, the results must be verified. To that end the results will be compared to the analytical predictions. In this case only the number density distribution is used.

Number Density at 4E-6s

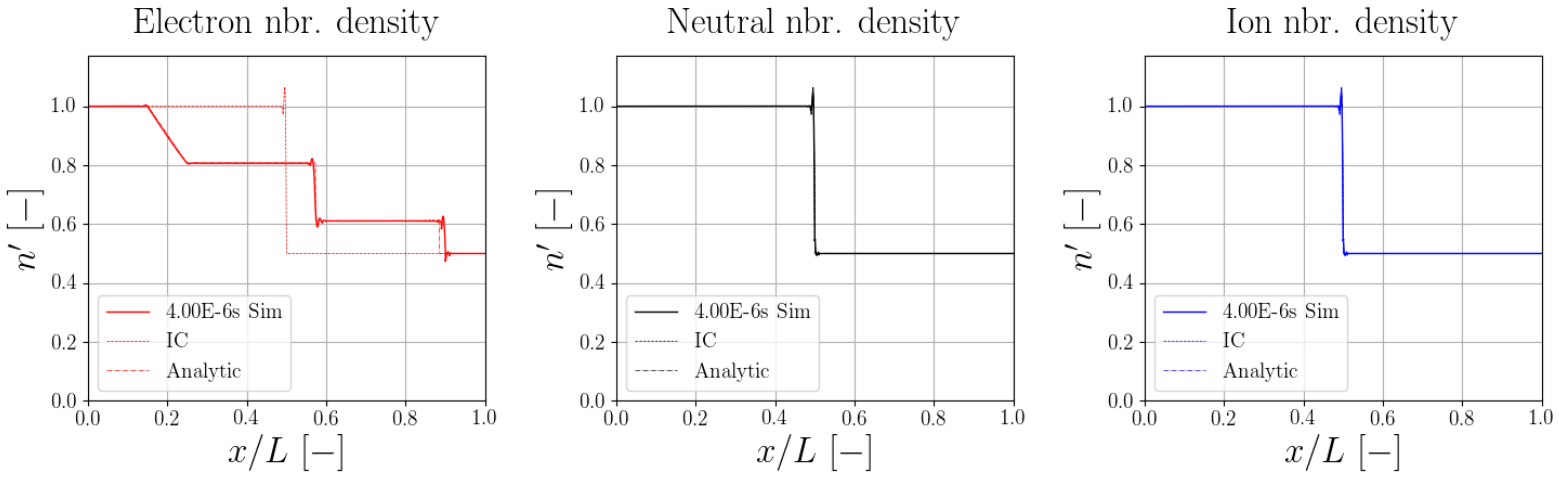

Figure 6.1: Number Density distribution at 4E-6s of the Euler-Like case.

At 4E-6s the prediction is that the discontinuities will have propagated for the electrons but there will be next to no change in the heavy species. This is also what is seen in the results from the simulation. The discontinuities are of the right type, the right change in variables and at the right places.

Number Density at 1.08E-3s

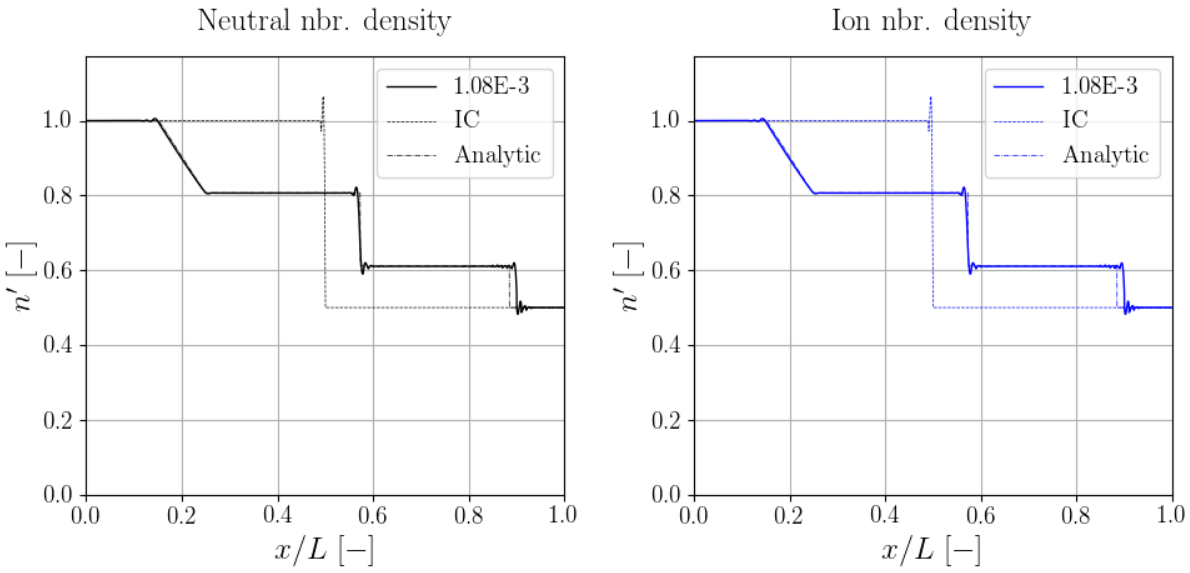

Figure 6.2: Number Density distribution at 1.08E-3s of the Euler-Like case. THe full lines are the result from the simulation, dotted lines are the Initial COnditions and dash dotted lines are the analytical solution.

At 1.08E-3s the distribution of the electrons was not predicted since the discontinuities have interacted with walls and each other making the analytical prediction very difficult. The Heavy species on the other hand have not gone through those events and were predicted. The simulations is conform to the prediction as it was for the electrons.

Overall the results are verified and thus the simulation can be used to study the effect of the multi-velocity non-dimensionalisation.

6.2 Improvement to the Model

As mentioned in the previous chapters of this work the new non-dimensionalisation brings two main improvements. The first is the relative scaling between the variables and thus the

level of precision of the results. The second is the convergence rate of the schemes.

The case used is a very simple one and thus measuring time to convergence or level of precision is difficult since the results are very good even with a worse non-dimensionalisation. That is why other criteria are used, as mentioned before.

6.2.1 Relative Scale of the Variables

The way the precision can be studied is through the relative scale of the different variables. Indeed if there is too large a disparity in the order of magnitude of the variables then the lower ones will not be resolved as precisely than the others.

The main culprit in this is the momentum of the electrons. Those variables are too high in the single velocity scaling compared to the other variables.

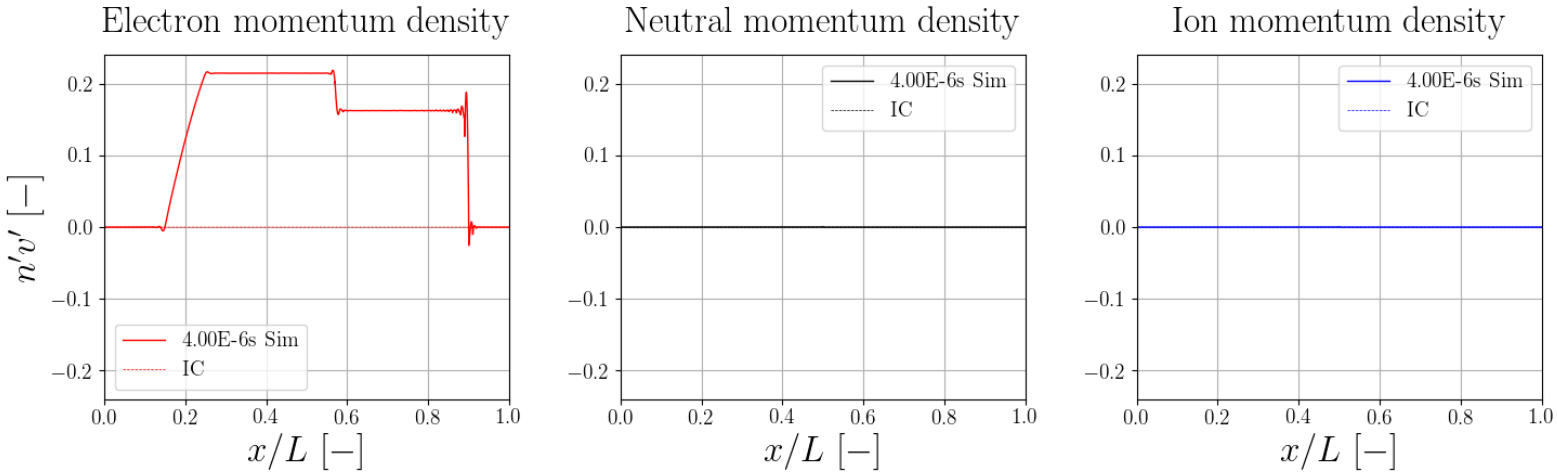

Figure 6.3: Momentum Density distribution at 4.00E-6s of the Euler-Like case with multi velocity scaling.

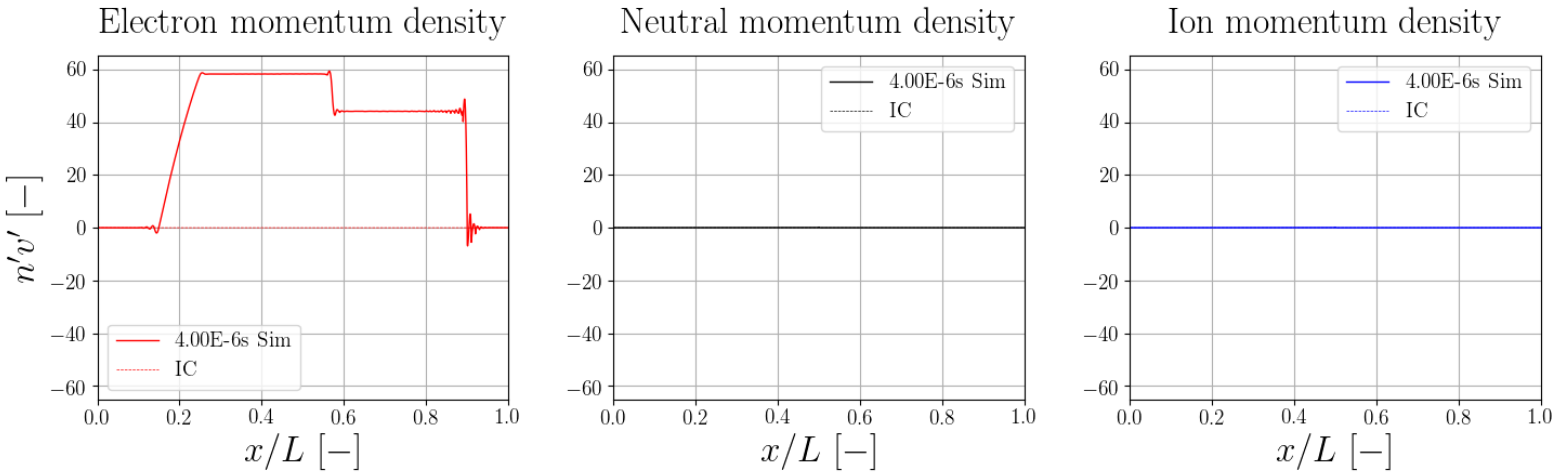

Figure 6.4: Momentum Density distribution at 4.00E-6s of the Euler-Like case with single velocity scaling.

As showed in Fig.6.3 and Fig.6.4 the multi velocity scaling brings the momentum variable of the electrons within the range of the other variables.

	Maximum value of Largest Variable	Maximum value of Smallest Variable	Ratio
Single Velocity Scaling	59.18	1	59.18
Multi Velocity Scaling	1.50	0.22	7.5

Table 6.1: Comparison of the highest and lowest values amongst the variables during the simulation.

6.2.2 Convergence Rate

Convergence rate is dependent on the ellipse $\mathcal{E}$ that contains the spectrum σ of $\mathbf{A}$, the expanded Jacobian. Specifically the center should be far and the semi-major axis small. For purely real eigenvalues this means that the ratio of the distance between the furthest eigenvalues of the distance to the middle of the values should be minimized. For complex values it means a spectrum that is not centered on the origin of the complex plane with a balance between a small semi-major axis and large excentricity.

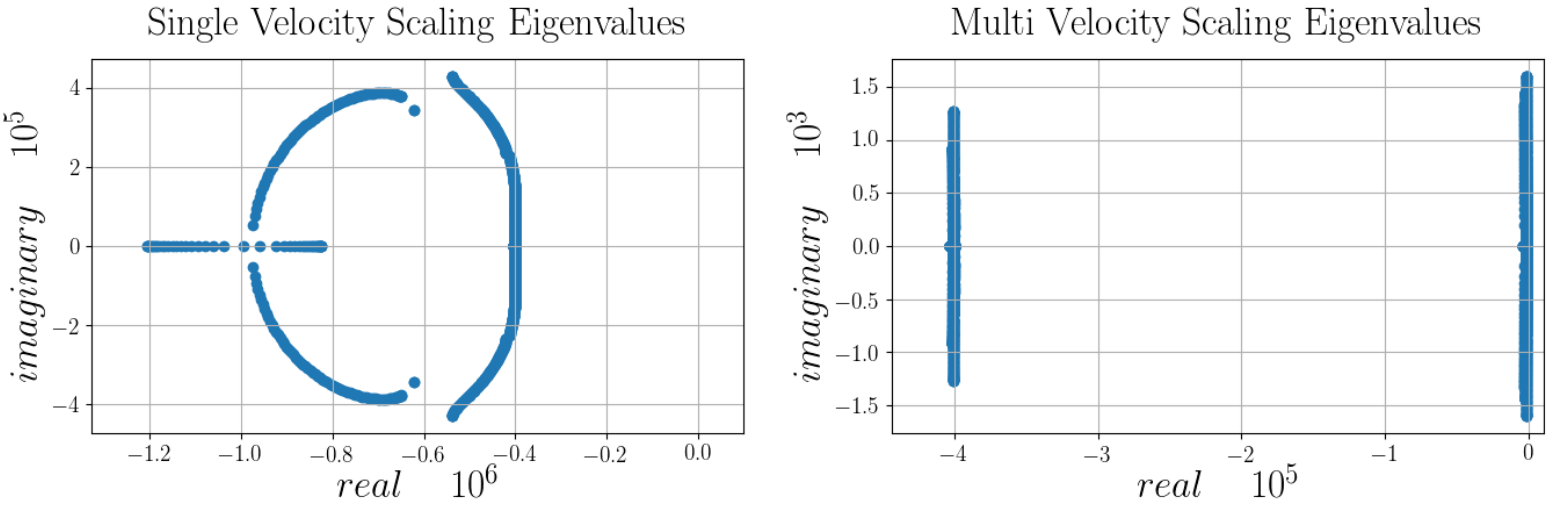

Figure 6.5: Eigenvalues of the expanded Jacobian for the single velocity scaling (left) and multi velocity scaling (right). Take note that the axes are not scaled in the same way.

Fig.6.5 shows that the multi velocity scaling results in much more clustered eigenvalues. As can be seen the real parts of the values are significantly smaller and thus much more clustered. This will result in a faster convergence rate as intended.

	Single Velocity Scaling	Multi Velocity Scaling
Largest Real Part	1.46E+6	4.03E+5
Smallest Real Part	4.00E+5	1.21E+3
Distance between min & max	1.06E+6	4.02E+5
Root Mean Square	4.42E+5	2.67E+5

Table 6.2: Comparison of the eigenvalues spectrum of the single and multi velocity scalings for the Euler-Like test case.

As mentioned in section 3.2.2 the conditioning should minimize the distance between the eignevalues and maximize the distance from the origin. To that end the maximum and minimum real parts and the root mean square have been computed. Tab.6.2 shows that the multi velocity scaling, while having a root mean square 0.6 times smaller, the distance between its minimum and maximum values is 2.64 times smaller.

The Euler-Like test case has shown the gains of the multi velocity scaling, the next test case, the acoustic system with electric potential test case, will add an aspect to the model, that of electric potential.

Chapter 7

Sod Shock Tube with Acoustic System and Electric Potential

This case is similar to the Euler-Like case. The difference being the presence of the electric potential. This has no effect on the other variables in this test. This case has for objective to test the computation of the electric potential in conjunction with the other variables, not it's effect on the other variables.

7.1 Validation of the Results

As with the previous test case, the results are verified using the analytical solution computed earlier.

Number Density is one of the two criteria used to validate the result since it displays 3 shocks unlike energy or pressure. This result is aligned with the analytical predictions in both the values in the different regions and the position of the discontinuities.

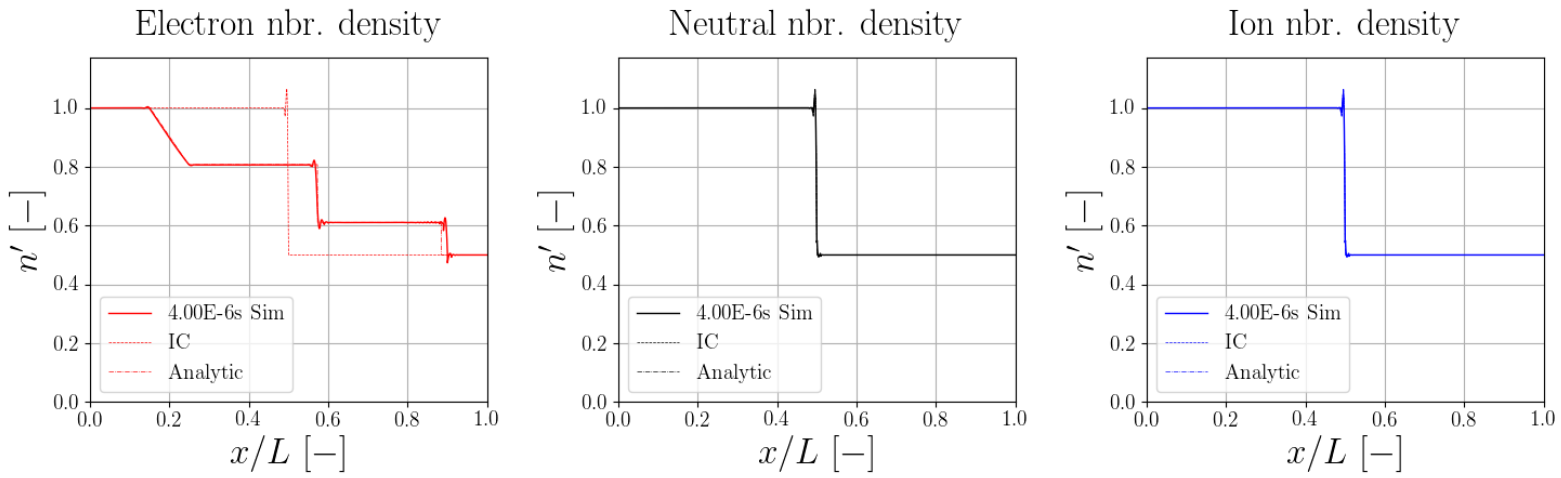

Figure 7.1: Number Density of electrons distribution at 4E-6s of the acoustic system with electric potential case.

Electric Potential The electric potential is the second criteria. It is also the shape expected by the analytical solution. As predicted the first derivative on the borders is the same. The issue being that the first derivative on the borders should be zero but is not exactly zero.

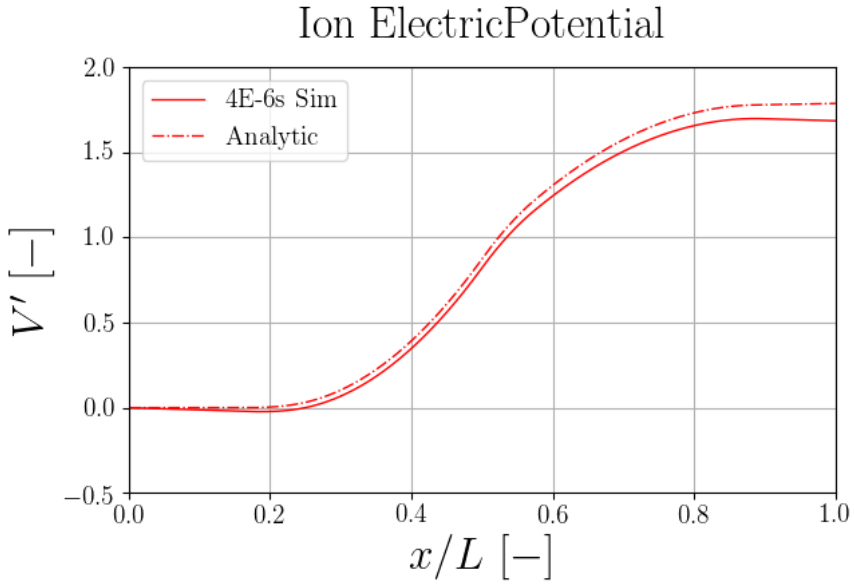

Figure 7.2: Electric Potential distribution at 4E-6s of the acoustic system with electric potential case.

The result is very close to the analytical solution as can be seen in Fig7.2. This verifies the result and suggest that it can be studied further. Additionally the value of interest is not that of the electric potential but its first derivative. This aspect is very closely satisfied notably the boundary condition. A probable source for the error relies in the slight oscillations around the shocks which are not physical.

What is possible to see is that the scaling of the electric potential is coherent with the other variables having a maximum value around 1.7.

7.2 Improvement to the Model

7.2.1 Relative Scale of the Variables

Just like for the Euler-Like case, the single velocity scaling presents the problem of having a variable much larger than the others. The addition of the electric potential does not change this since it is scaled to be in range with the other variables as shown in Fig.7.2.

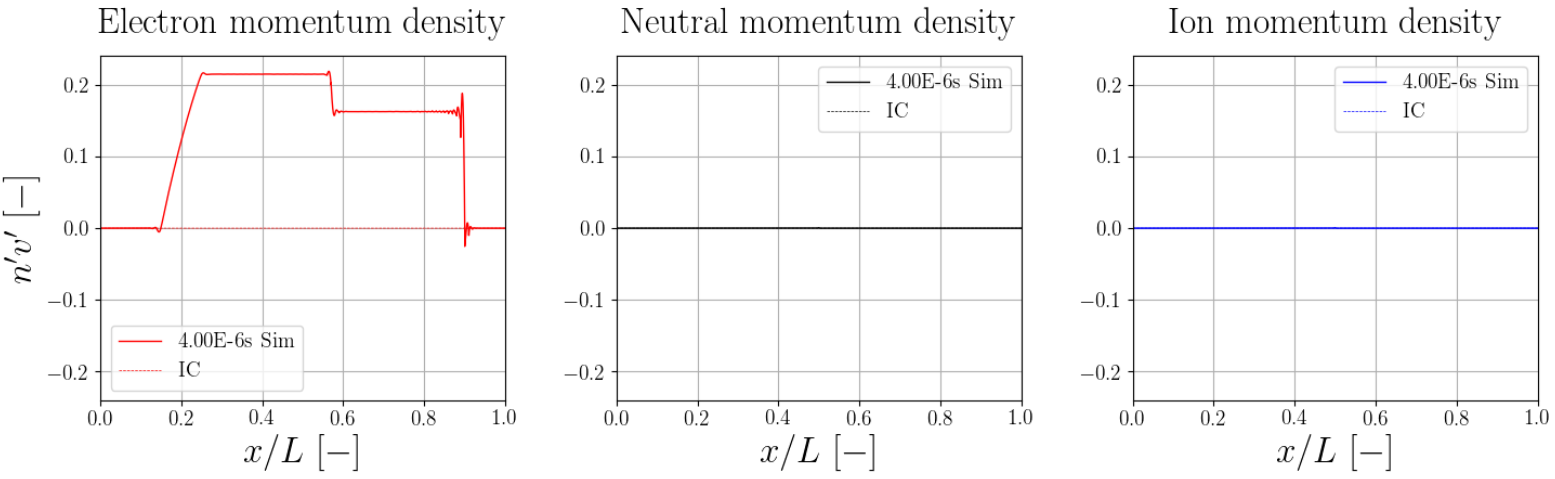

Figure 7.3: Momentum Density distribution at 4.00E-6s of the acoustic system with electric potential case with multi velocity scaling.

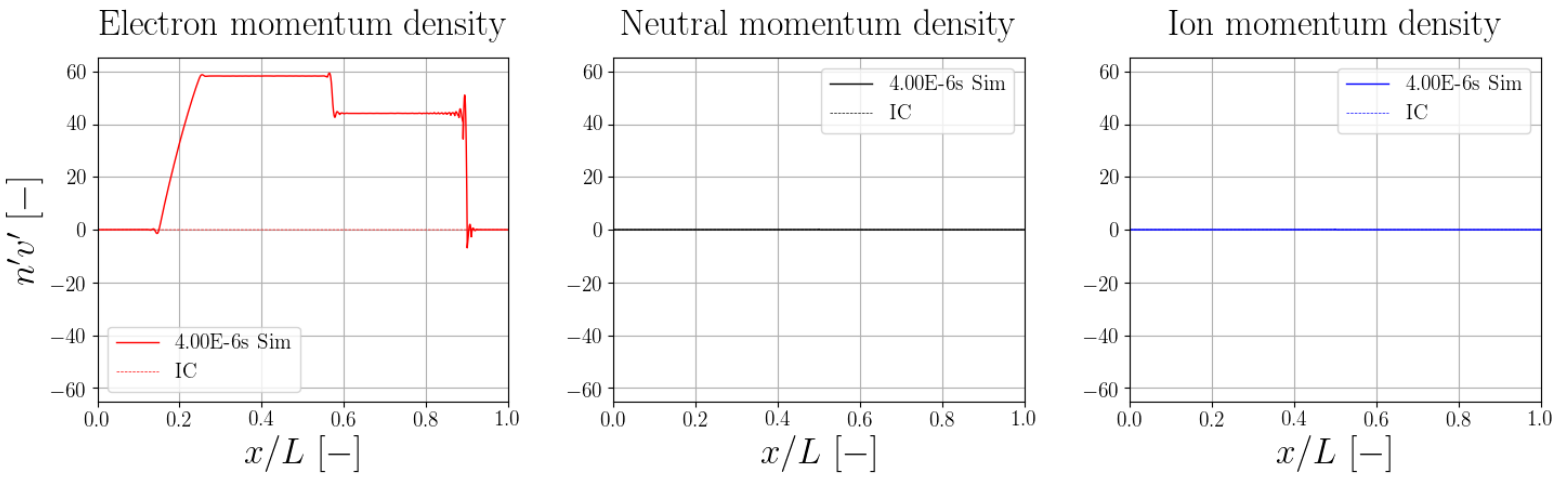

Figure 7.4: Momentum Density distribution at 4.00E-6s of the acoustic system with electric potential case with single velocity scaling.

As with the Euler-Like case the rescaling has brought the momentum within range of the other variables, insuring that it will not dominate the convergence calculation. This improves the precision of the other variables. This is evident when looking at the electric potential

7.2.2 Comparison of Electric Potentials

When looking at the electric potentials side by side it is obvious that one has to be incorrect. The multi velocity scaling result is much closer, almost identical in fact, to the analytical solution. This indicates that even when converging the single velocity scaling seems to not be able to find the correct electric potential. An error as large as this one requires further study to confirm its origin. Only a small part of the error must come from the inaccuracies in the density computation since that error would also be present for the multi velocity scale simulation and is suspected to the source of its small error.

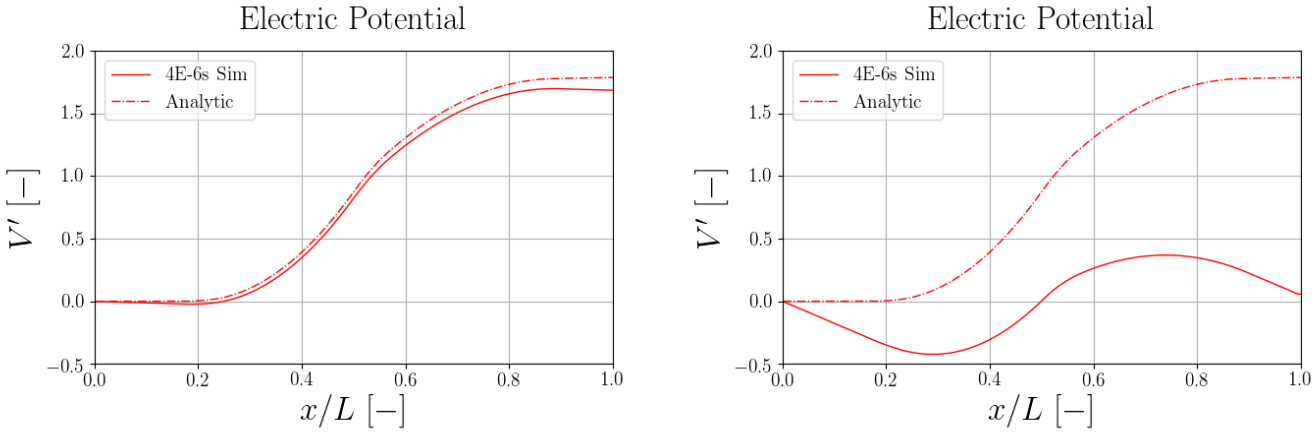

Figure 7.5: Comparison of the electric potential distribution at 4.00E-6s of the of the multi velocity scaling (left) and single velocity scaling (right).

It is also significant that the boundary condition of a zero first derivative at the right border of the domain is not respected at all by the single velocity scaling simulation even though convergence was within the same tolerance as the multi velocity scaling simulation. The most likely cause is that which was mentioned in section 3.1. The electron momentum density is so much larger than the other variables that it makes it so that their convergence has less weight resulting in erroneous results.

Such a large error would result in a greatly erroneous computation of the electric field. This field is the basis for the computation of the sources originating from electrical forces. This means that if this error remains, the single velocity scaling will not be able to be used for models that include electrical forces. This is a second reason to continue investigating the source of the error in the future.

7.2.3 Convergence Rate

It would be pointless to compare the convergence rate of a correct solution and an incorrect one. A much stricter convergence requirement and smaller time steps might lead the single velocity scaling to have correct results but this would of course increase computation time significantly.

Part IV

Future Work

Chapter 8

Future Test Cases

The cases that have been studied for this report are not the only tests that will be useful to determining the validity of the model. Several aspects have not been tested yet but will have to be.

8.1 Purpose

Gauge terms are already implemented but will have to be verified rather than the use of manually input BC as in the acoustic test case.

Sources originating from the electric potential are also already implemented but must still be validated. Indeed the acoustic case computes the electric potential but does not includes its effect on the other variables.

Chemistry is an aspect of plasma modeling that was not delved into in this work. The different species of particles interact through chemical reactions and can be both reactant and product, changing the overall amount of particles of each species. These reactions also have an impact on the momentum and energy of each species.

Alternate scaling schemes are being considered. In the current cases the multi velocity scaling seems appropriate and has shown to be an improvement on the single velocity scaling. But this does not mean that there are no other schemes more suited to other cases. This is why non-dimensionalisation schemes such as one based on source terms or outside electric potential are being considered.

8.2 Two Stream Perturbation

The two stream perturbation case is one where a sine wave of density of all species moves at a fixed speed. Using periodic BC it is possible to study the evolution of all the variables in an unsteady but predictable environment that is more challenging than the acoustic test case.

This test can make use of both gauge terms and the sources originating from electric potential. The inclusion of source terms for the momentum and energy will have significant impact on the Jacobian and thus its eigenvalues. This will once again test the clustering of the eigenvalues and show the improvement from the multi velocity scaling over the single velocity scaling.

8.3 Argon Reactor

The Argon Reactor test case is a test case specifically designed to test the chemical aspect of the model. It is 0D rather than 1D, there is no movement, just chemical interactions. This will test the number density and energy variables' chemical source terms.

8.4 Plasma Relaxation

The plasma relaxation test case is the case where the simulation follows a shock through gas, specifically argon3. This shock generates high temperatures that result in ionization of the gas. This test case regroups all of the past, present and future capabilities of the plasma side of the ForDGe software.

This case will bring together all the physics from previous cases and add the final terms: momentum and energy exchange between species and heat diffusion. This will complete the model and test all of its capabilities.

In addition to the new features this will be the final test of the multi velocity scaling. It will show if the new non-dimensionalisation is favorable when the full model is used. More than that it will also be the perfect test case to test other non-dimensionalisation such as one based on source terms.

8.5 Other Cases

Other test cases will be developed based on future work and results to test more non-dimensionalisation schemes, determining the best scheme depending on the application.

Chapter 9

Future Applications

9.1 Ablative shielding

Ablative shielding works by emitting plasma and gasses from the shielding to form a layer of cooler fluid around the space-craft during reentry. This process involves plasma and chemistry. That is why the development of a tool to model those events is important to the development of this technology [16].

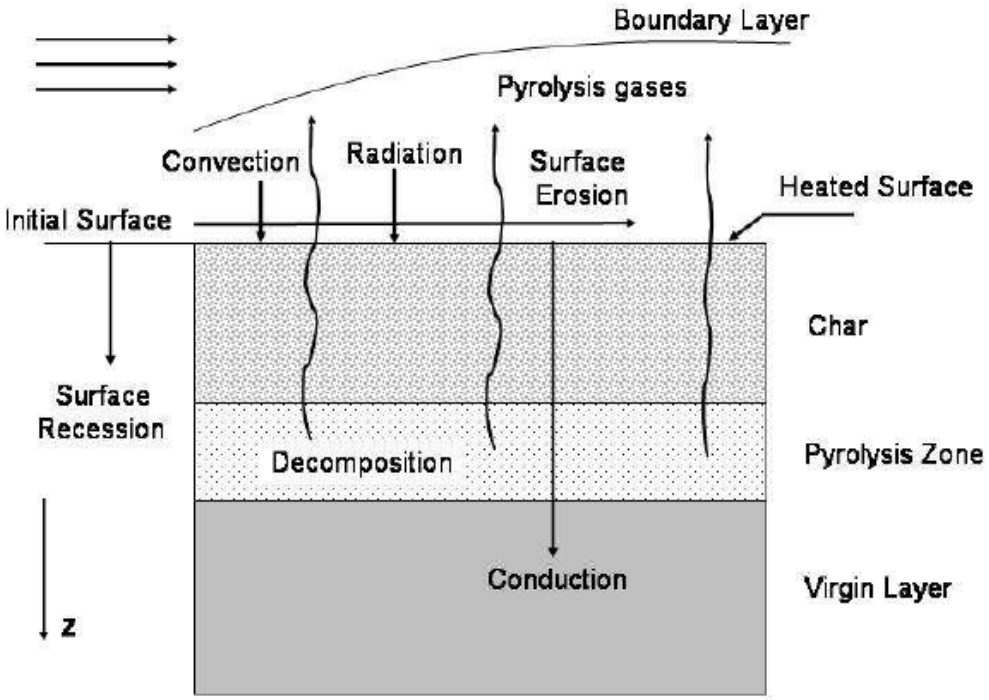

Figure 9.1: Ablative shielding diagram [17]

As shown in Fig.9.1 the heat of reentry makes the outer layer of the heat shield undergo pyrolisis. This phenomenon expels gasses and plasma. This layer insulates the spacecraft from heat due to friction. It can not be modeled satisfactorily by common computational fluid dynamics software. It requires chemistry and electrical forces to be properly modeled. This is why the addition of these features to ForDGe is beneficial.

9.2 Hall thruster

Electric thrusters such as the Hall Effect Thrusters are a heavily researched topic [13]. They do not provide the high thrust that chemical engines provide but their specific impulse, that is the amount of ΔV with respect to the mass of the fuel, is orders of magnitude larger than that of chemical engines.

That is the reason why such thrusters are used currently and why they are being researched. The development of a tool that could facilitate such research is therefor very desirable.

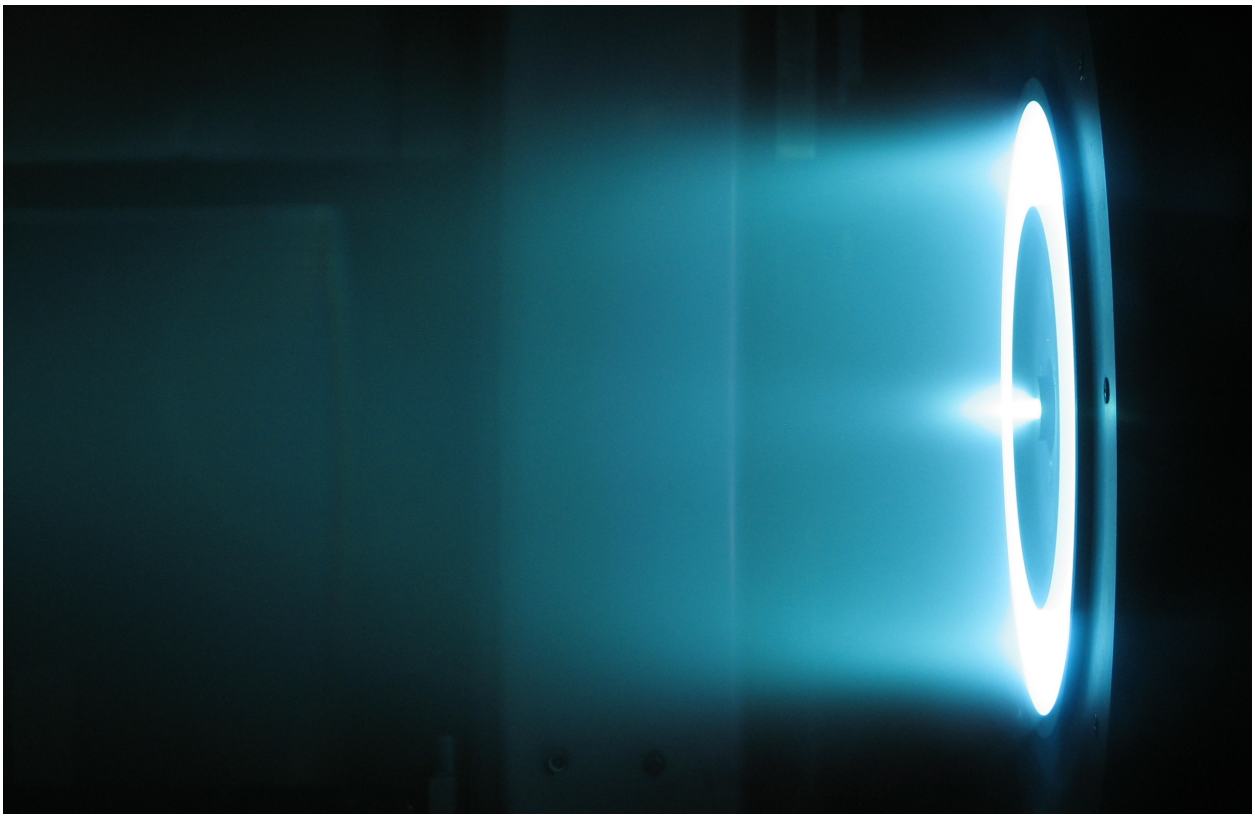

Figure 9.2: Xenon hall thruster, Courtesy of NASA/JPL-Caltech.

Hall thrusters rely on electric (and magnetic) effects to function, that is why a specialised

tool is necessary. Those forces are present to favor ionisation in the thruster, hence why all those capabilities are aimed for in the development of ForDGe.

Conclusion

This work is not the end of a research project, this work is but a step in the development of a tool capable of modeling plasma fluid mechanics. It started as an attempt to improve the conditioning of the plasma problem which is complex by it's nature, having such different particles as electrons and ions.

It has resulted not only in an improvement of the performances but added capabilities. Indeed while the primary goal was improving precision and convergence rate, which was accomplished, the added benefit was the added capability of computing the electric potential.

Adding the physics related to the electric potential, its diffusion and source term, was always an objective of this work. The fact that the improved conditioning was necessary for a correct computation of the electric potential was not expected but serves to illustrate the importance of the conditioning.

Moreover, the framework used to allow for a choice of non-dimensionalisation is now put in place and flexible, meaning that additional non-dimensionalisation schemes can easily be added. The ability to choose the conditioning based on the problem being solved will be very valuable in the future.

The next step of development is clear, there are still aspects of plasma physics that are not implemented but are required for the modeling of a wide range of cases. In order to be able to model cases such as ablative shielding, hall thrusters and more, it will be necessary to have access to chemical and electrical sources for the number density, momentum density and energy density variables.

To conclude, this is an important step in the development of a plasma modeling tool but the road ahead is still long and promising.

Bibliography

[1] J C Adam et al. "Physics, simulation and diagnostics of Hall effect thrusters". In: *Plasma Physics and Controlled Fusion* 50.12 (Dec. 1, 2008), p. 124041. ISSN: 0741-3335, 1361-6587. DOI: 10.1088/0741-3335/50/12/124041. URL: https://iopscience.iop.org/article/10.1088/0741-3335/50/12/124041 (visited on 01/05/2023).

[2] A. Alvarez Laguna et al. "An asymptotic preserving well-balanced scheme for the isothermal fluid equations in low-temperature plasmas at low-pressure". In: *Journal of Computational Physics* 419 (Oct. 2020), p. 109634. ISSN: 00219991. DOI: 10.1016/j.jcp.2020.109634. URL: https://linkinghub.elsevier.com/retrieve/pii/S0021999120304083 (visited on 12/12/2022).

[3] Alejandro Alvarez Laguna. *Multi-fluid modeling of magnetic reconnection in solar partially ionized and laboratory plasmas*. von Karman Institute for Fluid Dynamics, 2018. ISBN: 978-2-87516-130-7. DOI: 10.35294/phdt201803. URL: https://store.vki.ac.be/vkiphdt201803-alvarez-laguna.html (visited on 12/12/2022).

[4] F Bassi et al. "INVESTIGATION OF HIGH-ORDER TEMPORAL SCHEMES FOR THE DISCONTINUOUS GALERKIN SOLUTION OF THE NAVIER-STOKES EQUATIONS". In: ().

[5] F. Bassi et al. "High-order accurate p-multigrid discontinuous Galerkin solution of the Euler equations". In: *International journal for numerical methods in fluids* 60.8 (2009). Place: Chichester, UK Publisher: John Wiley & Sons, Ltd, pp. 847–865. ISSN: 0271-2091.

[6] M. S. Benilov. "A kinetic derivation of multifluid equations for multispecies nonequilibrium mixtures of reacting gases". In: *Physics of Plasmas* 4.3 (Mar. 1997), pp. 521–528. ISSN: 1070-664X, 1089-7674. DOI: 10.1063/1.872151. URL: http://aip.scitation.org/doi/10.1063/1.872151 (visited on 12/12/2022).

[7] Amaury Bilocq et al. "Hybridization of Discontinuous Galerkin methods for shock capturing in scale resolving simulations". In: event-place: Oslo, Norway. F.R.S.-FNRS - Fonds de la Recherche Scientifique [BE], June 8, 2022.

[8] Philipp Birken. "Numerical methods for the unsteady compressible Navier-Stokes equations". In: ().

[9] N Corthouts. "Travail de Fin d'Etudes :€Discontinuous Galerkin Finite Element Method Applied to Plasma Flows". In: ().

[10] F Custinne. "Master thesis and internship[BR]- Master's thesis : Plasma sheath modeling with a high order Discontinuous Galerkin Method[BR]- Integration internship". In: ().

[11] Koen Hillewaert. "Development of the discontinuous Galerkin method for high-resolution, large scale CFD and acoustics in industrial geometries". In: ().

[12] J. Jara-Almonte, N. A. Murphy, and H. Ji. "Multi-fluid and kinetic models of partially ionized magnetic reconnection". In: *Physics of Plasmas* 28.4 (Apr. 2021), p. 042108. ISSN: 1070-664X, 1089-7674. DOI: 10.1063/5.0039860. URL: https://aip.scitation.org/doi/10.1063/5.0039860 (visited on 12/12/2022).

[13] I. Levchenko et al. "Perspectives, frontiers, and new horizons for plasma-based space electric propulsion". In: *Physics of Plasmas* 27.2 (Feb. 2020), p. 020601. ISSN: 1070-664X, 1089-7674. DOI: 10.1063/1.5109141. URL: http://aip.scitation.org/doi/10.1063/1.5109141 (visited on 01/05/2023).

[14] Randall J. LeVeque. *Numerical methods for conservation laws*. 2nd ed. Lectures in mathematics ETH Zürich. Publication Title: Numerical methods for conservation laws. Basel: Birkhäuser verlag, 1992. ISBN: 3-7643-2723-5.

[15] Abner J. Salgado and Steven M. Wise. *Classical Numerical Analysis: A Comprehensive Course*. 1st ed. Cambridge University Press, Oct. 31, 2022. ISBN: 978-1-108-94260-7 978-1-108-83770-5. DOI: 10.1017/9781108942607. URL: https://www.cambridge.org/core/product/identifier/9781108942607/type/book (visited on 12/12/2022).

[16] Pierre Schrooyen et al. "Fully implicit Discontinuous Galerkin solver to study surface and volume ablation competition in atmospheric entry flows". In: *International Journal of Heat and Mass Transfer* 103 (Dec. 2016), pp. 108–124. ISSN: 00179310. DOI: 10.1016/j.ijheatmasstransfer.2016.07.022. URL: https://linkinghub.elsevier.com/retrieve/pii/S0017931015310127 (visited on 01/05/2023).

[17] Balaji Venkatachari et al. "Computational Tools for Re-Entry Aerothermodynamics: Part II. Surface Ablation". In: Jan. 2008. ISBN: 978-1-62410-128-1. DOI: 10.2514/6.2008-1218.

Part V

Appendices

Appendix A

Runge-Kutta Butcher's Tableau

A.1 Explicit of Order 4

0	0	0	0	0
1/2	1/2	0	0	0
1/2	0	1/2	0	0
1	0	0	1	0
	1/6	1/3	1/3	1/6

Table A.1: Coefficients for the Explicit Runge-Kutta of order 4 scheme. [8]

A.2 Explicit Single Diagonal Implicit Runge-Kutta

0	0	0	0	0	0	0
1/2	1/4	1/4	0	0	0	0
83/250	$\frac{8611}{62500}$	$\frac{-1743}{31250}$	1/4	0	0	0
31/50	$\frac{5012029}{34652500}$	$\frac{-654441}{2922500}$	$\frac{174375}{388108}$	1/4	0	0
17/20	$\frac{15267082809}{155376265600}$	$\frac{-71443401}{120774400}$	$\frac{730878875}{902184768}$	$\frac{2285395}{8070912}$	1/4	0
1	$\frac{82889}{524892}$	0	$\frac{15625}{83664}$	$\frac{69875}{102672}$	$\frac{-2260}{8211}$	1/4
	$\frac{82889}{524892}$	0	$\frac{15625}{83664}$	$\frac{69875}{102672}$	$\frac{-2260}{8211}$	1/4

Table A.2: Coefficients for the Explicit Single Diagonal Implicit Runge-Kutta 64 scheme. [8]